

Dear Editor of *Geoscientific Model Development*,

We thank the reviewers for their support and their comments. We have modified the manuscript according to these comments and queries and we think that these changes have largely improved our manuscript. Accordingly, the main points that were modified refer to:

- (1) The reference versions of the ocean surface albedo scheme as well as the reference version of the two atmosphere models are now clearly displayed in the revised manuscript in agreement with <http://www.geosci-model-dev.net/8/3487/2015/gmd-8-3487-2015.html>
- (2) Updated or revised figures that now includes CMIP5 results to clearly show the large differences in simulated ocean surface albedo
- (3) Improved text including new references related to previously developed ocean surface albedo scheme

Please find a detailed response to each questions/comments point by point below in [blue](#) (text fragments are *in blue italics*).

#### **Anonymous Referee #1**

Received and published: 21 July 2017

The authors present an interactive ocean surface albedo scheme that is based on pulling together results from previously published studies. Nevertheless, for the two atmospheric models (AGCMs) that is applied to it represents a substantial improvement. The presentation has a clear layout and comprises the development of the scheme itself, its implementation in the AGCMs, evaluation of the analytical results, evaluation against observations (both remotely sensed and ground-based), and finally an evaluation of its performance in the AGCMs against the previously used schemes. While there are still obvious shortcomings of the new scheme, which the authors discuss, it still represents a very clear improvement.

In my view, the ms. is excellent with regards to all four review criteria for GMD. I will suggest a few points for improving the ms. below; these constitute a minor review in my opinion.

[We thank the reviewer for his/her support.](#)

#### 1) General remarks

I am wondering whether it could be interesting to compare the OSA parametrization developed here to other state-of-the art AGCMs, given that the previously used schemes in LMDZ and ARPEGE were somewhat outdated. Since the authors work within the CRESCENDO framework, they might want to

consider some of the other AGCMs used in CRESCENDO for that purpose.

We appreciate this suggestion and we choose to include in Figure 7 the results from other CMIP5 models. Figure 7 confirms that there are large differences (and thus uncertainties) in simulated ocean surface albedo across CMIP5 models, including ARPEGE-Climat and LMDZ (used in the CNRM-CM and IPSL-CM climate models, respectively).

We also revise Figure 4 to include the Payne (1972) ocean albedo formulation which is used in several state-of-the-art Earth system models.

Section 6. The comparison with the ground-based data (Fig. 6) shows a large discrepancy in the albedo PDF around the value of 0.06. While the authors discuss the general problems of comparing a model grid-cell average with observed point values in the last paragraph of section 6, I would think that this feature deserves more explanation. Perhaps the modelled peak in the PDF is flatter in higher-resolution model runs?

Figure 6 was provided to support our explanations on model-data discrepancy at COVE station. Using a high resolution of ARPEGE-Climat (T359 that offers a horizontal resolution of about 50 km), we find that model resolution does not impact the distribution of direct and diffuse shortwave radiations (Figure R1). Although the horizontal resolution can change the climate dynamics and hence some drivers of the OSA such as wind speed and cloudiness, the numerical representation of the radiative scheme remains unchanged in the current version of the high-resolution model. This is why the distribution of direct and diffuse shortwave radiations is similar to that of the model version used in the submitted manuscript. As a consequence, we decide to not include this comparison in the revised manuscript.

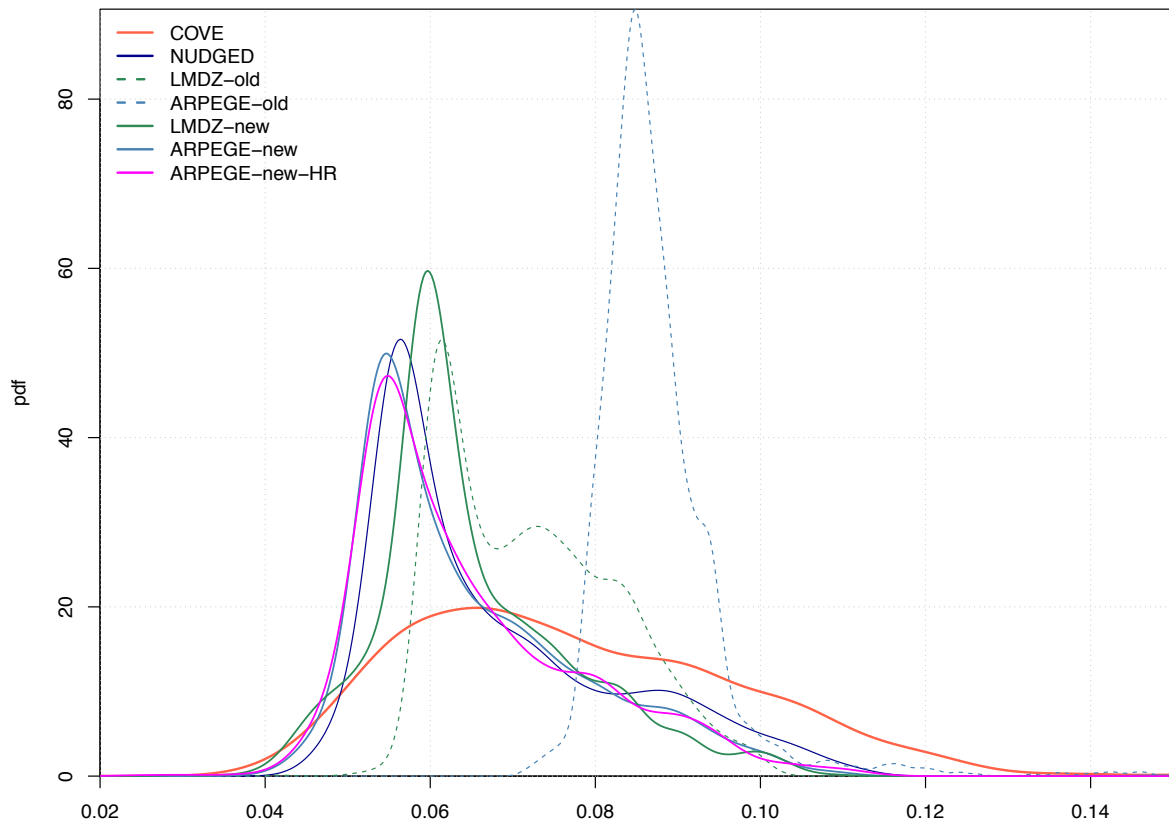


**Figure R1:** Probability density function of daily-mean ocean surface albedo at COVE station (36.905°N, 75.713°W) derived from daily-mean time series over years 2001 to 2013. Ocean surface albedo derived from ground-based observations and as reconstructed with ARPEGE-Climat nudged toward Era-Interim are indicated in red and dark blue, respectively. Ocean surface albedo simulated by ARPEGE-Climat (in blue) and LMDZ (in green) using old or the new interactive scheme are indicated with dashed or solid lines, respectively. ARPEGE-Climat-HR (T359; 50km horizontal resolution) is given with a magenta solid line.

## 2) Specific remarks

I.102 This paragraph needs updating to reflect the current structure of the ms.

The text has been revised accordingly (please refer to the track-change version of the manuscript).

I.346 "i.e." I think "e.g." fits better here.

Taken into account in the revised manuscript

Figure 4: the legend in the panels needs updating with regards to the referenced papers.

Taken into account in the revised manuscript



## **Anonymous Referee #2**

Received and published: 25 August 2017

General Comments: The manuscript presents a new scheme for computing ocean surface albedo (OSA), and evaluates the scheme in two numerical models. While the existing suite of OSA schemes consider variations only due to solar zenith angle, the new scheme considers the various processes that contribute to the overall albedo. These processes include reflection by the ocean surface free of whitecaps, reflection by the ocean surface covered with whitecaps, and the reflection of solar energy that first passes downward through the air-sea interface is scattered within the ocean and then passes back through the air-sea interface to the atmosphere. Additionally, the study considers direct and diffuse irradiance separately as they can have very different OSA values due to their difference in angular distributions (via dependence of OSA on solar zenith angle). Spectral variations are also considered. In summary, the new parameterization incorporates the relevant physics. In that sense, there is scientific merit to the improved parameterization.

[We thank the reviewer for his/her support.](#)

To judge a broader scientific merit, the change in the skill of climate simulations that use the new OSA parameterization must be evaluated. This is not performed in the study. Rather, the manuscript indicates it will be performed in a subsequent study. The new scheme is justified by showing it gives OSA values that are much closer to observations than the old scheme. This is well and good, but isn't it the skill of climate parameters with societal influence (such as air temp, rainfall, storm frequency, etc.) that are the greatest importance? While the improved scheme gives OSA values that better match observations, the scientific merit of the scheme can only truly be judged once it is shown the improved scheme elevates the skill of models in simulating parameters beyond OSA. Ideally, this study would be published in conjunction with a study giving a broader evaluation of the new scheme's impact on climate simulations.

[We truly believe that the description of a new interactive ocean albedo scheme and its evaluation against available modern observations should remain the scope of the manuscript. Further investigations relate to the impact of the OSA scheme on the atmospheric fields or climate fields would require a set of dedicated experiments because each parameterization of the ocean surface albedo would imply a different adjustment of the atmospheric model in particular in terms of its global radiative balance. As mention in Hourdin et al. \(2017\) or Schmidt et al. \(2017\), the calibration or tuning of atmospheric model is highly complex and non-linear. Any change in the atmospheric parameterization such as the ocean surface albedo would ultimately impact the radiative imbalance](#)

of the model. Therefore, comparing the impact of various ocean albedo is not straightforward and requires a set of dedicated simulations and analysis to clearly attribute a changes in climate fields to a given parameterization of OSA and not to a model drift as shown in (Gupta et al., 2013). We expect that forthcoming reference publications ARPEGE-Climat and LMDZ in the context of CMIP6 will document the impact of the ocean albedo scheme and that of other improved atmospheric physical parameterizations on the simulated climate.

Along these same lines, it's not clear what, exactly, motivates the study. Climate model upgrades are typically motivated by the need to improve some aspect of climate model simulations, such as reducing a regional temperature bias (for example the warm bias in the eastern tropical Pacific). The Introduction indicates that OSA interacts with bio- physical processes, OSA receives little attention, and OSA parameterizations don't include all the underlying physics. While not clearly stated, it seems like the study is motivated by the fact that existing OSA albedo parameterizations are dated and there is now sufficient computer power for including more computationally intense OSA schemes. The lack of connection to overall climate model skill detracts from the overall scientific quality.

The development of numerical models for weather prediction and climate simulation is traditionally driven by both the need to reduce known model biases and shortcomings and the incorporation of better physics as our understanding improves. A model with small biases (because of a parametrization very well fitted to the observations) could still miss an important feedback mechanisms under climate change because of important missing physics. It is important that both these bottom-up and top-down motivations be recognized as being important. In the case of OSA, the rationale for including better physics, keeping in mind the large spread of OSA in CMIP5 models discussed above, is rather clear.

The science is presented in a clear and organized manner that allows for reproducibility. In the broad sense, the presentation quality is high. The paper is well organized and generally clear. However, the manuscript could be improved with additional attention to detail. The manuscript discusses a broad range of topics from details of ocean optics to atmospheric model specifics and results. Given inconsistencies and inaccuracies, primarily in the OSA parameterization development sections of the paper, it appears author expertise is in climate modeling and not ocean optics. In addition, there are some key references neglected in the work (indicated below).

We thank the reviewer for this recommendation; these references are now included and acknowledged in the revised manuscript.

Despite the criticisms above, OSA schemes in the existing suite of climate models do not reflect state-of-the-art knowledge of OSA physics (as the manuscript correctly indicates). A thorough evaluation of the sensitivity of climate models to OSA is not known to exist. It could be argued there is scientific merit to improving the representation of the underlying physics represented in climate models (this is not clearly done in the manuscript; one could also argue that hindcast skill is the only thing that matters). By presenting an improved OSA scheme, the authors are opening a door to further investigations of the sensitivity of climate model results to OSA.

Specific Comments (#'s 1, 2 and 3 are fairly significant):

- 1) Upper ocean models still largely utilize OSA values presented by Payne (1972; Albedo at the Sea Surface, JAS). Given the paucity of albedo observations, the authors are encouraged to evaluate their improved scheme in the context of the Payne (1972) values as well as the COVE station values considered in the manuscript.

We thank the reviewer for this suggestion. We revise Figure 4 accordingly including Payne (1972) formulation which is used in several state-of-the-art Earth system models. However, Payne (1972) formulation for ocean surface albedo does not differ much from that of Taylor et al. (1996), we chose to only discuss this alternative parameterization in section 3. (Please refer to the track-change version of the manuscript).

- 2) The OSA scheme being presented is referred to as an “interactive” OSA. It’s not clear exactly what “interactive” means or why that term is necessary.

We use this wording to contrast with previous schemes that use ad hoc formulations to simulate ocean surface albedo. These ad hoc formulations such as Payne (1972), Taylor et al. (1996) or Larsen et al. (1977) only derive the ocean surface albedo from zenith solar angle (an exogenous quantity to the model) whereas a number of others physical quantities (simulated by the model) can influence its global scale distribution.

In our scheme, the ocean surface albedo responds to (i.e. interact) with atmospheric radiation (direct and diffuse) thanks to the spectral dependence (across a range of wavelengths between 200 and 4000 nm). It also depends on the ocean surface characteristics dictated by surface winds, chlorophyll content and whitecaps. It provides a much more physical basis to resolve the radiative transfer at the interface between the atmosphere and the upper ocean, and enable coupling between earth system model components like surface ocean wave or marine biogeochemistry.

3) There is a two-part series of papers published by Ohlmann and Siegel (2000; JPO) that parameterize OSA in terms of solar zenith angle, cloud forcing (i.e. direct vs diffuse light), and chlorophyll concentration. That scheme captures similar physics to the one presented in this manuscript with the exception of whitecaps and appears computationally more efficient than the scheme presented. Could it be adapted for use in climate models. If so, how does it compare? If not, why?

We thank the reviewer for bringing up relevant literature. Work published by Ohlmann and Siegel (2000) is definitely in the scope of our paper. We therefore acknowledge this work in the revised manuscript and clearly state that our code compares well in terms of complexity to HYDROLIGHT.

Regarding the other question, we think that comparing various albedo schemes is not the scope of this work. Li et al. (2006) have used the Canadian atmosphere model as a framework to test various ocean albedo scheme but do not test Ohlmann and Siegel (2000) [maintained now as HYDROLIGHT].

Besides, implementing and testing a new code in two different models would require a significant amount of time and also availability of the source code. Unfortunately, this is not the case for HYDROLIGHT which is under commercial license (see page 10 of <http://www.commtec.com/Prods/mfgs/Sequoia/brochures/hydrolight.pdf>).

4) Abstract indicates “precise OSA calculation without penalizing the model elapsed time”. However conclusion states a 2% increase in elapsed model run time. While 2% is small, it is technically a penalty to run time.

We apologize for this mistake. The accurate numbers is 0.2% which better corresponds to our statement. We have corrected the manuscript accordingly.

5) Line 57. Incorrect statement. Photosynthesis is not necessarily directly related to the amount of solar radiation.

We apologize for this incorrect statement. We have reworded the sentence as follows:

*“OSA also influences a number of biogeochemical processes such as the photosynthesis or photolysis, which respond to incoming solar radiation within the upper-lit layer of the ocean.”*

6) Line 130. Should be “direct and diffuse”.

Taken into account.

7) Line 167. The clear water absorption coefficient for  $\lambda < 400$  nm is set to zero “due to lack of available data”. Smith and Baker (1981; Applied Optics) present data that are available but not considered.

We thank the reviewer for his/her suggestion. However, this subsection relates to the reflectance of whitecaps and not the optical properties of clear water between 200 and 400 nm. To our knowledge, there is no recent update of the whitecap reflectance as published by Whitlock et al. (1982).

We would like to stress that the table provided in the supplementary material shows all coefficients used in our scheme including values between 200 and 4000 nm, that may include Smith and Baker (1981) estimates. Therefore, unless stated otherwise (as in line 167 of the submitted manuscript) used coefficients are applicable from 200 to 4000 nm.

8) Below water albedo (Line 229) is not a technically correct quantity given “surface” (OSA) albedo includes a contribution from this term. What is referred to as below water albedo is technically irradiance reflected back to the atmosphere by the ocean interior that contributes to OSA. Further (line 232) the manuscript states it has multiple reflections, but technically only a single reflection is necessary.

We thank the reviewer for his/her suggestion. We have change the wording in the manuscript and the figures accordingly. We hope the new wording is more accurate in the revised version of the manuscript.

9) Line 234. It is stated that DOM “can influence radiative properties in the ocean” but the authors go on to neglect it in their parameterization. Neglecting DOM because chlorophyll has the largest impact is not justification. The authors should be clear as to why DOM is neglected (the corresponding signal in OSA is relatively small, parameterizations based on DOM don’t exist).

We appreciate reviewer comment. We amend the text as follows:

*“Previous studies show that DOM can influence radiative properties of the open ocean (e.g., Behrenfeld and Falkowski, 1997; Dutkiewicz et al., 2015; Kim et al., 2015). However, we chose to solely account for the influence of the marine biological pigment which is characterized by its chlorophyll content because the influence of DOM on ocean surface albedo is expected to be small compared to that of surface chlorophyll.”*

10) A nomenclature is defined/utilized where a indicates the various OSA components. For the “surface” component the superscript s is used, for the “below water” component the superscript w is used. But then for the “whitecap” component, the wc is given as a subscript. Making wc a superscript would improve consistency with other terms.

We thank the reviewer for his/her suggestion. We move wc as a subscript accordingly.

11) Line 505 indicates “old OSA schemes are unable to capture seasonal variations as observed”. Technically neither the new nor the old schemes capture the observed seasonal cycle exactly. The point is that the new scheme does a better job of capturing the seasonal cycle than the old scheme. The manuscript should clarify this.

We thank the reviewer for his/her useful comment. We have amended the text accordingly and include further discussed related to the revised Figure 7 (which now include CMIP5 results). The revised text is given below:

*“At seasonal scale, OSA estimated from averaged radiative fluxes agrees with the above-mentioned findings for ground-based observations and models. Figure 7 clearly shows that old OSA schemes do not capture seasonal variations of observed OSA. Correlation between observation-derived OSA and that simulated by both models is 0.32 for ARPEGE-Climat and 0.28 for LMDZ, which is very low, indicating an unrealistic representation of OSA. Comparison with CMIP5 atmosphere models shows that OSA as simulated by ARPEGE-Climat or LMDZ are in the range of CMIP5 models (0.04–0.17), confirming the large uncertainties related to simulated OSA in state-of-the-art climate model. While several CMIP5 models replicate seasonal variation in OSA, most of them exhibit large biases in simulated OSA compared to the observation-based estimate. Only ACCESS1-3, BNU-ESM, HadCM3, MIROC-ESM and MIROC-ESM-CHEM display a mean seasonal cycle of OSA comparable to the observation-based estimate at COVE station. For ARPEGE-Climat, this erroneous representation of OSA at seasonal scale leads, at least for this location, to a systematic bias in the surface energy budget of  $+3 \text{ W m}^{-2}$  in winter and  $-1.5 \text{ W m}^{-2}$  in summer. It is thus likely that large deviation in OSA as simulated by CMIP5 lead to substantial errors in energy flow at the air-sea interface.*

*Figure 7 shows significant improvements in the simulated OSA in both models using the new interactive scheme. In both models, the simulated seasonal cycle of OSA replicates the minimum observed during the summer. Although using the new interactive OSA scheme, both models do not capture large values of OSA of 0.10 occurring during the winter. That said, model-data comparison shows that correlation with observations has been improved. Indeed, correlation between observed*

*and simulated daily values over a mean yearly cycle has increased from 0.23 to 0.84 in LMDZ to 0.32 to 0.86 in ARPEGE-Climat.”*

12) Line 610 indicates a “better coupling between atmosphere and ocean components”. Technically the study only demonstrates that the new OSA scheme enables an improved air-sea exchange of solar radiation.

We appreciate the reviewer’s comment. The text has been revised accordingly.

13) The Larsen et al. (1972) reference in Figure 4 is missing from the reference list. It’s possible that the Figure 4 label should be Larsen and Barkstrom (1977).

Taken into account in the revised manuscript

#### References

- Gupta, A. Sen, Jourdain, N. C., Brown, J. N., & Monselesan, D. (2013). Climate drift in the CMIP5 models. *Journal of Climate*, 26(21), 8597–8615. [https://doi.org/10.1175/JCLI\\_D\\_12\\_00521.1](https://doi.org/10.1175/JCLI_D_12_00521.1)
- Hourdin, F., Mauritsen, T., Gettelman, A., Golaz, J.-C., Balaji, V., Duan, Q., ... Williamson, D. (2017). The Art and Science of Climate Model Tuning. *Bulletin of the American Meteorological Society*, 98(3), 589–602. <https://doi.org/10.1175/BAMS-D-15-00135.1>
- Schmidt, G. A., Bader, D., Donner, L. J., Elsaesser, G. S., Golaz, J. C., Hannay, C., ... Saha, S. (2017). Practice and philosophy of climate model tuning across six US modeling centers. *Geoscientific Model Development*, 10(9), 3207–3223. <https://doi.org/10.5194/gmd-10-3207-2017>

1 **An interactive ocean surface albedo scheme (OSAv1.0): formulation and**  
2 **evaluation in ARPEGE-Climat (V6.1) and LMDZ (V5A)**

Supprimé: two atmospheric models

3  
4 **Roland Séférian<sup>1\*</sup>, Sunghye Baek<sup>2,3</sup>, Olivier Boucher<sup>2</sup>, Jean-Louis Dufresne<sup>4</sup>, Bertrand**  
5 **Decharme<sup>1</sup>, David Saint-Martin<sup>1</sup>, Romain Roehrig<sup>1</sup>**

6 <sup>1</sup> Centre National de Recherches Météorologiques, Météo-France/CNRS, Toulouse, France

7 <sup>2</sup> Institut Pierre-Simon Laplace, CNRS / UPMC, Paris, France

8 <sup>3</sup> Now at Korea Institute of Atmospheric Prediction Systems (KIAPS), Seoul, Korea

9 <sup>4</sup> Laboratoire de Météorologie Dynamique, CNRS / UPMC, Paris, France

10  
11 **Abstract**

12  
13 Ocean surface represents roughly 70% of the Earth surface, playing a large role in the  
14 partitioning of the energy flow within the climate system. The ocean surface albedo (OSA) is  
15 an important parameter in this partitioning because it governs the amount of energy  
16 penetrating into the ocean or reflected towards space. The old OSA schemes in the ARPEGE\_  
17 Climat and LMDZ models only resolve the latitudinal dependence in an *ad hoc* way without  
18 an accurate representation of the solar zenith angle dependence. Here, we propose a new  
19 interactive OSA scheme suited for Earth system models, which enable coupling between earth  
20 system model components like surface ocean wave or marine biogeochemistry. This scheme  
21 resolves spectrally the various contributions of the surface for direct and diffuse solar  
22 radiation. The implementation of this scheme in two Earth system models leads to substantial  
23 improvements in simulated OSA. At the local scale, models using the interactive OSA scheme  
24 better replicate the day-to-day distribution of OSA derived from ground-based observations in  
25 contrast to old schemes. At global scale, the improved representation of OSA for diffuse  
26 radiation reduces model biases by up to 80% over the tropical oceans, reducing annual-mean  
27 model-data error in surface upwelling shortwave radiation by up to 7 W m<sup>-2</sup> over this domain.  
28 The spatial correlation coefficient between modelled and observed OSA at monthly resolution  
29 has been increased from 0.1 to 0.8. Despite its complexity, this interactive OSA scheme is

Supprimé: which gather contributions for relevant OSA processes published in the literature over the last decades.



33 computationally efficient to enable precise OSA calculation without penalizing the model  
34 elapsed time.

35

36

### 37 1- Introduction

38 The surface radiation budget has long been recognized as fundamental to our understanding of  
39 the climate system (IPCC, 2001; 2007; 2013). The flow of radiative energy through the Earth  
40 System and the radiative interactions between the atmosphere and the ocean remain one of the  
41 major sources of uncertainties in climate predictions (Allen et al., 2009; Frölicher, 2016;  
42 Gillett et al., 2013; Myhre et al., 2015; Otto et al., 2013).

43

44 In the atmosphere, the spatiotemporal variations in incoming solar radiation and its  
45 atmospheric absorption drive the hydrological cycle as well as the flow of air masses. In the  
46 oceans, the fraction of solar radiation entering in subsurface is controlled by the oceanic  
47 surface albedo (OSA). The corresponding amount of heat stored into the ocean constitutes an  
48 important term in the ocean energy surface balance and affects in turn the whole climate  
49 system. On short (daily to seasonal) time scales, solar radiation absorbed into the upper-ocean  
50 layers affects the stability of the ocean mixed layer, the sea surface temperature and may, in  
51 turn, influence the geographic structure of large-scale atmospheric convection (Gupta et al.,  
52 1999). Over longer time scales, the fraction of energy entering into the ocean contributes to  
53 increase the ocean heat content, which is key term to diagnose the climate sensitivity from  
54 observations (Otto et al., 2013).

55

56 OSA interacts with a multitude of biophysical processes occurring in the first meters of the  
57 ocean. In particular, it governs the amount of solar radiation entering in the upper-most layer  
58 of the ocean that interacts with marine biological light-sensitive pigment like chlorophyll, and  
59 other materials in suspension (e.g., Morel and Antoine, 1994; Murtugudde et al., 2002). OSA  
60 also influences a number of biogeochemical processes such as the photosynthesis or  
61 photolysis, which respond to incoming solar radiation within the upper-lit layer of the ocean.

62 Conversely, penetrating ultraviolet solar radiation can also produce detrimental impacts on the  
63 marine biota (e.g., Li et al., 2014; Smyth, 2011). Consequently, OSA influences marine  
64 primary productivity directly, and hence ocean ecosystems and ocean carbon uptake (e.g.,  
65 Behrenfeld and Falkowski, 1997; Nelson and Smith, 1991; Siegel et al., 2002).

66

**Supprimé:** is directly related to the amount of

**Supprimé:**

**Supprimé:** available

70

71 Despite its importance, OSA is a parameter that often receives insufficient attention from both  
72 observational and modelling points of view. Most of the available data are indirectly retrieved  
73 from satellite observations of the top-of-atmosphere radiative budget (Wielicki et al., 1996),  
74 with relatively few direct observations of surface radiative fluxes. Nonetheless, the OSA  
75 processes are relatively well understood so that OSA can be parameterized at the global scale.

76

77 Both empirical and theoretical approaches indicate that the solar zenith angle (SZA) is the  
78 single most prominent driving parameter for OSA. However a wide range of other parameters  
79 such as the partitioning of incoming solar radiation between its direct and diffuse components,  
80 the sea surface state (often approximated through the surface wind), the concentration of  
81 suspended matter and plankton light-sensitive pigment in the surface ocean, and the extent  
82 and physical properties of whitecaps also affect OSA. All of these contributions vary  
83 spectrally and OSA thus depends on the spectral distribution of the incoming solar radiation at  
84 the surface (Jin, 2004; Jin et al., 2002).

85

86 Over the last decades, several schemes have been proposed to model OSA (e.g., Cox and  
87 Munk, 1954; Hansen et al., 1983; Kent et al., 1996; Larsen and Barkstrom, 1977;  
88 Preisendorfer and Mobley, 1986; [Ohlman, Siegel and Mobley, 2000](#)). Some schemes depend  
89 only on the solar zenith angle while others additionally depend on quantities like wind speed  
90 or cloud optical depth, inducing substantial differences in OSA patterns and variability. Li et  
91 al. (2006) investigated the impact of various OSA schemes in the Canadian atmosphere  
92 climate model, AGCM4. The authors show that the difference in clear-sky upwelling  
93 shortwave radiation between schemes can reach  $20 \text{ W m}^{-2}$  at the top-of-the-atmosphere and  
94 more than  $20 \text{ W m}^{-2}$  at the surface.

95

96 Most of the schemes assessed in Li et al. (2006) do not resolve spectral variations in OSA  
97 thus excluding the possibility to represent subtle processes and couplings in Earth system  
98 models [as suggested by complex ocean radiative transfer \(e.g., Ohlman, Siegel and Mobley,  
99 2000; Ohlman and Siegel, 2000\)](#). Indeed, changes in whitecaps and ocean color, whether due  
100 to climate variability or climate change, can modify the OSA, with potential impacts on  
101 photochemistry in the atmosphere and biological activity in the upper-most layer of the ocean  
102 (Hense et al., 2017).

103

104 In this study, we propose a new interactive OSA scheme well-adapted for the current  
105 generation of Earth system models which may benefit from and benefit to the coupling  
106 between earth system model components like surface ocean wave or marine biogeochemistry.  
107 This study provides details of its implementation into two atmospheric models and discusses  
108 its performance on daily to seasonal time scales.

109

110 The outline is as follows. In Section 2, we introduce the formulation of the interactive OSA  
111 scheme which is derived from old schemes published in literature over the last decades. In  
112 Section 3, we analyze the importance of the various components of this scheme using a stand-  
113 alone version of the OSA scheme. Section 4 describes the experimental design and the two  
114 state-of-the-art atmospheric models that are used in Sections 5, 6 and 7 to evaluate the  
115 interactive OSA scheme against available observations. Section 8 concludes the present study.

Supprimé: based on

Supprimé: Assessment of the simulated OSA in two atmosphere models in comparison to available observations is detailed in Section 4

Supprimé: 5

116

## 117 2- Interactive Ocean Surface Albedo parameterization

118 Albedo is a measure of the reflectivity of a surface and is defined as the fraction of the  
119 incident solar radiation that is reflected by the surface. It depends not only on the properties of  
120 the surface but also on the properties of the solar radiation incident on that surface.  
121 Technically-speaking albedo can be computed from the knowledge of the spectral and  
122 directional distribution of the incident solar radiation  $L(\lambda, \theta, \varphi)$  and the bidirectional  
123 reflectance distribution function (BRDF),  $\rho(\lambda, \theta_i, \varphi_i, \theta_r, \varphi_r)$  which links the reflected radiation in  
124 a direction  $(\theta_r, \varphi_r)$  to that of incident radiation in a direction  $(\theta_i, \varphi_i)$ . Here,  $\lambda$  represents the  
125 wavelength, and  $(\theta, \varphi)$  the zenith and azimuthal angles.

126 While the atmospheric incident radiation,  $L(\lambda, \theta, \varphi)$ , can be solved using a radiative transfer  
127 model and the BRDF can be modelled from the knowledge of the surface ocean properties,  
128 the complexity and the computational cost of such models are prohibitive for climate  
129 applications. Thus, estimation of OSA in climate models has to rely on several simplifying  
130 assumptions. In particular, incident solar radiation is usually characterized by a downward  
131 direct flux (for which SZA is known) and a diffuse downward flux (for which a typical  
132 angular distribution can be assumed).

133 In the present work, most of the analytic formulations employed are derived from the  
134 azimuthally averaged radiative transfer equation (Chandrasekhar, 1960), enabling a  
135 straightforward estimation of the OSA for direct and diffuse radiation. This implies that zenith  
136 solar angle is the only directional parameter involved in the parametrization.

142

143 The suite of processes involved in our scheme is displayed in Figure 1. The incident solar  
144 radiation (either direct and diffuse) is first influenced by the presence of foam (composing the  
145 whitecaps), which exhibits different reflective properties from sea-water. Then, the reflective  
146 properties of the uncapped fraction of the sea surface are determined separately for direct and  
147 diffuse incident radiation. Finally, the subsurface —or ocean interior— reflectance of sea  
148 water is computed for both direct and diffuse incident radiation.

Supprimé: or

Supprimé: below-water

149

150 Hereafter, we describe the various components of OSA according to the nature of the incident  
151 solar radiation (direct or diffuse) and the processes involved in its reflection.

152

### 153 2-1 Treatment of whitecaps

154 The first contribution to the new interactive OSA scheme is the whitecap cover. Indeed, the  
155 whitecap albedo,  $\alpha^{WC}(\lambda)$ , could significantly increase the OSA at high wind speeds (e.g.,  
156 Frouin et al., 2001; 1996; Gordon and Wang, 1994; Stramska, 2003).

Supprimé:  $\alpha_{WC}$

157 The presence of whitecaps originates from turbulence induced by the breaking of waves,  
158 which generates foam at the sea surface (Deane and Stokes, 2002; Melville and Matusov,  
159 2002). In the absence of an ocean wave model such as WAM (e.g., Aouf et al., 2006; Ardhuin  
160 et al., 2010) which would provide a more accurate whitecap coverage ( $WC$ ) based on wave  
161 significant height (Bell et al., 2013; Woolf, 2005), we used the formulation of  $WC$  published  
162 in Salisbury et al. (2014). Their expression is based on recent space-borne observations with a  
163 37 GHz channel radar. It parametrizes  $WC$  as a function of the 10-meter wind speed,  $w$ , in  
164 unit of  $\text{m s}^{-1}$ :

$$165 \quad WC(w) = 3.97 \cdot 10^{-2} w^{1.59}$$

166 As mentioned in Salisbury et al. (2014), this approximation of  $WC$  is valid for  $w$  ranging  
167 between 2 and 20  $\text{m s}^{-1}$ , which corresponds well to the range of  $w$  values simulated by the  
168 current generation of Earth system models. The formulation employed here does not account  
169 for temperature dependence of wave-breaking in agreement with other parameterizations for  
170  $WC$  (Stramska, 2003) because its effect is weaker than that of surface winds on the whitecaps  
171 coverage.

172 In order to solve the spectral dependence of the whitecap albedo, we use the relationship  
173 proposed by Whitlock et al. (1982). Yet, we rely on previous work indicating that the  
174 whitecap albedo of ordinary foam,  $\alpha^{WC}(\lambda)$ , tends to be twice lower than that of fresh and

Supprimé:  $\alpha_{WC}$

179 dense foam (Koepke, 1984). We consequently apply a  $\frac{1}{2}$  coefficient to the formulation  
180 proposed by (Whitlock et al., 1982) for  $\alpha_{WC}(\lambda)$  from 400 to 2400 nm, as follows:

181  $\alpha^{WC}(\lambda)$

$$182 = \frac{1}{2} \times \frac{1}{100} (60.063 - 5.127 \ln r_{WC}(\lambda) + 2.779 (\ln r_{WC}(\lambda))^2 - 0.713 (\ln r_{WC}(\lambda))^3$$

183  $+ 0.044 (\ln r_{WC}(\lambda))^4)$

184 where  $r_{WC}$  is the absorption coefficient of clear water in  $m^{-1}$ . We use  $r_{WC}(\lambda)$  as published in  
185 Whitlock et al. (1982) from 400 to 2400 nm. Outside the 400 to 2400 nm range, we chose to  
186 set  $r_{WC}(\lambda)$  to zero due to the lack of available data in the literature. Tabulated values of  
187  $\alpha^{WC}(\lambda)$  computed using this assumption are provided in Table S1.

188 In the present scheme, we assume that whitecaps reflect equally direct and diffuse incoming  
189 solar radiation. We also assume that our formulation, which is based on observations, is not  
190 affected by the small contribution from the subsurface reflectance.

191

192

## 193 2-2 Treatment of the uncapped surface

### 194 2-2-1 Fresnel surface albedo for direct radiation

195 We describe the contribution of Fresnel reflection at the ocean surface, which is a major  
196 component of the OSA. Fresnel reflection is assumed to depend at a given wavelength,  $\lambda$ , on  
197 the solar zenith angle,  $\theta$  and the refractive index of sea water ( $n$ ), and the two-dimensional  
198 distribution of the ocean surface slopes,  $f$ . As mentioned earlier we neglect the dependence  
199 on the azimuthal angle of the incident radiation.

200 We follow Jin et al. (2001) and express the direct surface albedo ( $\alpha_{dir}^S$ ) as follows:

201

$$202 \alpha_{dir}^S(\lambda, \theta, w) = r_f(n(\lambda), \mu) - \frac{r_f(n(\lambda), \mu)}{r_f(n_0, \mu)} f(\mu, \sigma)$$

203

204 where  $\mu = \cos(\theta)$ ,  $n$  is the spectral refractive index of sea water,  $r_f$  is the Fresnel reflectance  
205 for a flat surface and  $f$  is a function that accounts for the distribution of multiple reflective  
206 facets at the ocean surface. Tabulated values for  $n(\lambda)$  are indicated in Table S1.  $n_0 = 1.34$   
207 corresponds to the refractive index of sea water averaged from 300nm to 700 nm (i.e., visible  
208 spectrum) for which the  $f$  function is estimated.

209

Supprimé:  $\alpha_{WC}$

Supprimé:  $\alpha_{WC}$

212 The interaction of incident shortwave radiation with the multiple reflective facets at the ocean  
 213 surface of various angle and direction is difficult to model. It is nonetheless possible to  
 214 represent statistically the distribution of slope of ocean reflective facets with a probabilistic  
 215 function. The probabilistic function provided by Cox and Munk (1954) assumes a Gaussian  
 216 distribution of mean slope facet as follows:

$$217 \quad p(\tan\vartheta) = \frac{1}{\pi\sigma^2} \exp\left(\frac{-\tan^2\vartheta}{\sigma^2}\right)$$

218 where  $\vartheta$  is the facet angle, i.e., the angle between the normal to the facet and the normal to the  
 219 horizontal ocean surface and  $\sigma$  the width the distribution of the facet angle. The parameter  $\sigma$ ,  
 220 also called the surface roughness, is modulated by the influence of surface (i.e. 10-meter)  
 221 wind speed ( $w$ ) as  $\sigma^2 = 0.003 + 0.00512 w$ . The formulation by Cox and Munk (1954)  
 222 assume that (1) shading influence of ocean facets is neglected and (2) ocean surfaces never  
 223 behave as a theoretical Fresnel surface (requiring  $\sigma = 0$ ). These approximations can impact  
 224  $\alpha_{dir}^S$  calculation at high SZA and/or in absence of winds. Besides, this formulation (based on  
 225 wind speed only) ignores the effect of the wind direction on the wind sea and the effect of  
 226 swell which both affect the distribution of slopes. This latter set of assumptions can also be  
 227 revised in the foreseeable future when climate models will include an interactive ocean wave  
 228 model.

229 In order to account for various impacts of multiple ocean surface facets to  $\alpha_{dir}^S$  including both  
 230 multiple scattering (increasing surface reflection) and shading effect (reducing reflection), Jin  
 231 et al. (2011) have proposed to express  $f$  as a polynomial function. This function intends to  
 232 parameterize the mean contribution of multiple reflective facets at the ocean surface to  $\alpha_{dir}^S$   
 233 using only the parameters  $\mu$  and  $\sigma$ . This polynomial function is expressed as:

$$234 \quad f(\mu, \sigma) \\
 235 \quad = (0.0152 - 1.7873\mu + 6.8972\mu^2 - 8.5778\mu^3 + 4.071\sigma - 7.6446\mu\sigma) \times \exp(0.1643 \\
 236 \quad - 7.8409\mu - 3.5639\mu^2 - 2.3588\sigma + 10.054\mu\sigma)$$

237 Coefficients of  $f$  have been fitted using several accurate calculations of  $\alpha_{dir}^S$  using a radiative  
 238 transfer model (Jin et al., 2006; 2005).

239

#### 240 **2-2-2 Fresnel surface albedo for diffuse radiation**

241 The amount and distribution of incident diffuse radiation strongly depend on the amount and  
 242 characteristics of cloud and aerosols. It is therefore difficult to derive an analytical  
 243 formulation for  $\alpha_{dif}^S$  from a BRDF that would be applicable to all atmospheric conditions. We

244 therefore choose to use the simple expression for the diffuse surface albedo ( $\alpha_{dif}^S$ ) under  
 245 cloudy sky proposed in Jin et al. (2011) which is:  
 246  $\alpha_{dif}^S(\lambda, w) = -0.1479 + 0.1502 n(\lambda) - 0.0176 n(\lambda)\sigma$   
 247 with  $\sigma$  and  $n$  defined as previously.

### 249 2-3 Contribution of the ocean interior reflectance to surface albedo

250 In this section, we describe the contribution of the ocean interior reflectance to the ocean  
 251 surface albedo,  $\alpha^W$ . It is caused by solar radiation penetrating the ocean but eventually  
 252 returning to the atmosphere after one or multiple reflections within the sea water volume.  
 253 Below the ocean surface, solar radiation interacts not only with sea water but also with  
 254 material in suspension in the water like the marine biological pigment or detrital organic  
 255 materials (DOM). Previous studies show that DOM can influence radiative properties of the  
 256 open ocean (e.g., Behrenfeld and Falkowski, 1997; Dutkiewicz et al., 2015; Kim et al., 2015).  
 257 However, we chose to solely account for the influence of the marine biological pigment which  
 258 is characterized by its chlorophyll content because the influence of DOM on ocean surface  
 259 albedo is expected to be small compared to the surface chlorophyll. Furthermore the  
 260 abundance of chlorophyll in sea water is monitored from space since decades (e.g.,  
 261 Behrenfeld et al., 2001; Siegel et al., 2002; Yoder et al., 1993) by so-called ocean color  
 262 measurements. Such observations can provide a climatology to use in the climate model in  
 263 absence of ocean biogeochemical module.

265 Over the uncapped ocean surface, the fraction of direct radiation penetrating into the upper-  
 266 most layer of the ocean  $1 - \alpha_{dir}^S$  interacts with the sea-water, which has a reflectance  $R_0$ .  
 267 Upwelling radiation can be reflected downward at the air-sea interface with a reflectance  $r_w$ .  
 268 Therefore, the contribution of multiple reflections of the penetrating radiation to the ocean  
 269 albedo takes the form of the following Taylor series:

$$270 \alpha^W(\lambda, \theta, Chl) = (1 - \alpha_{dir}^S)(1 - r_w)R_0(1 + r_w R_0 + (r_w R_0)^2 + (r_w R_0)^3 + \dots)$$

271 which can be arranged as follows:

$$272 \alpha^W(\lambda, \theta, Chl) = \frac{(1 - r_w)R_0}{1 - r_w R_0} (1 - \alpha_{dir}^S)$$

273 We employ the formulation of  $r_w$  and  $R_0$  proposed by Morel and Gentili (1991).

274 These authors express  $r_w$  as function of surface roughness  $\sigma$ , that is;  $r_w = 0.4817 -$   
 275  $0.0149\sigma - 0.2070\sigma^2$

Supprimé: Below-water albedo

Supprimé: below-water albedo

Supprimé: to the ocean surface albedo

Supprimé: While p

Supprimé: .

Supprimé: this has the largest impact at the global scale

Supprimé:

Supprimé:

284  $R_0$  represents an apparent optical property of sea water, which can be written as follows:

$$285 \quad R_0(\lambda, \eta, \mu, Chl) = \beta(\eta, \mu) \frac{0.5b_w(\lambda) + b_{bp}(\lambda, Chl)}{a_w(\lambda) + a_{bp}(\lambda, Chl)}$$

286 where  $a_w(\lambda)$  and  $b_w(\lambda)$  are the absorption and backscattering coefficients of sea water (in  $m^{-1}$ );  $a_{bp}(\lambda, Chl)$  and  $b_{bp}(\lambda, Chl)$  are absorption and backscattering coefficients of biological pigments (i.e., the chlorophyll).

289  $\beta(\eta, \mu)$  is function of sea water and biological pigment backscattering and can be written as:

$$290 \quad \beta(\eta, \mu) = 0.6270 - 0.2227\eta - 0.0513\eta^2 + (0.2465\eta - 0.3119)\mu$$

$$291 \quad \text{where } \mu = \cos(\theta) \text{ and } \eta = \frac{0.5b_w(\lambda)}{0.5b_w(\lambda) + b_{bp}(\lambda, Chl)}.$$

292 Backscattering of biological pigment,  $b_{bp}$ , is computed using the formulation proposed in  
293 Morel and Maritorena (2001) which uses chlorophyll concentration,  $[Chl]$ , as a surrogate of  
294 biological pigment concentration as follows:

$$295 \quad b_{bp}(\lambda) = 0.416[Chl]^{0.766} \left( 0.002 + \frac{1}{100} (0.50 - 0.25 \ln[Chl]) \left( \frac{\lambda}{550} \right)^{0.5(\ln[Chl]-0.3)} \right)$$

296 with  $\lambda$  expressed here in nm and  $[Chl]$  in  $mg\ m^{-3}$ . This formulation is valid for  $[Chl]$  ranging  
297 between 0.02 and 2  $mg\ m^{-3}$ .

298 The absorption of biological pigment,  $a_{bp}(\lambda, Chl)$ , is also computed using Morel and  
299 Maritorena (2001) formalism:

$$300 \quad a_{bp}(\lambda) = 0.06 a_{chl}(\lambda)[Chl]^{0.65} + 0.2(0.00635 + 0.06[Chl]^{0.65})e^{0.014*(440-\lambda)}$$

301 where  $a_{chl}(\lambda)$  is the absorption of chlorophyll in  $m^{-1}$  and  $\lambda$  and  $[Chl]$  as previously defined.

302

303 Previous estimates of  $a_{chl}(\lambda)$ ,  $a_w(\lambda)$  and  $b_w(\lambda)$  used in by Morel and Maritorena (2001)  
304 cover values for wavelengths ranging between 300 to 700 nm. Therefore, we have combined  
305 and interpolated several sets of tables of coefficients in order to solve consistently  $\alpha^W$ ,  $\alpha_{dir}^S$   
306 and  $\alpha_{dif}^S$  across the same range of wavelengths (i.e., from 200 to 4000 nm).  $a_w(\lambda)$  has been  
307 derived from tables provided by Smith (1982) and Irvine and Pollack (1968), which spans 200  
308 to 800 nm and 800 to 4000 nm, respectively.  $a_{chl}(\lambda)$  has been derived from values published  
309 in Frigaard et al. (1996) which differ from those in Morel and Maritorena (2001) (Figure 2).  
310  $b_w(\lambda)$  is estimated from sea water backscattering coefficients published in (Morel and  
311 Maritorena, 2001) that have been interpolated from 300 to 700 nm to 200 to 4000 nm with  
312 polynomial splines. Tabulated values for  $a_{chl}(\lambda)$ ,  $a_w(\lambda)$  and  $b_w(\lambda)$  are given in Table S1.

313



314

315 The difference in the contribution of the ocean interior reflectance to the ocean surface albedo  
316 for direct and diffuse essentially stems from the incident direction of incoming radiation. In  
317 the case of ocean interior reflectance for direct incoming radiation,  $\alpha_{dir}^W, \mu = \cos(\theta)$  whereas  
318 in the case of ocean interior reflectance for diffuse,  $\alpha_{dif}^W, \mu = 0.676$ . This value is considered  
319 as an effective angle of incoming radiation of  $47.47^\circ$  according to Morel and Gentili (1991).  
320 Hence  $\alpha_{dif}^W(\lambda, Chl) = \alpha_{dir}^W(\lambda, \arccos(0.676), Chl)$ .

Supprimé: between  
Supprimé: below-water albedo  
Supprimé: direct below-water albedo  
Supprimé: diffuse below-water albedo

321

## 322 2-5 Computation of OSA

323 With the various components of OSA being now parameterized, the OSA for direct and  
324 diffuse radiation are estimated as follows:

325  $OSA_{dir}(\lambda, \theta, w, Chl) = (\alpha_{dir}^S(\lambda, \theta, w) + \alpha_{dir}^W(\lambda, \theta, Chl))(1 - WC(w)) + WC(w)\alpha_{dir}^{WC}(\lambda)$

Supprimé:  $\alpha_{wc}$

326  $OSA_{dif}(\lambda, \theta, w, Chl) = (\alpha_{dif}^S(\lambda, w) + \alpha_{dif}^W(\lambda, Chl))(1 - WC(w)) + WC(w)\alpha_{dif}^{WC}(\lambda)$

Supprimé:  $\alpha_{wc}$

327

328 Since detailed atmospheric radiative transfer (e.g., Clough et al., 2005; Mlawer et al., 1997)  
329 are now part of current generation of Earth system models, most of radiative codes resolve  
330 radiation from near-ultraviolet ( $\sim 200$  nm) to near-infrared ( $\sim 4000$  nm) wavelengths. Here, we  
331 design our scheme to compute both the spectral and broadband OSA. To this effect, the  
332 scheme computes the OSA from  $\lambda_1 = 200$  to  $\lambda_2 = 4000$  nm with a resolution of 10 nm. The  
333 contribution of each wavelength interval  $d\lambda$  to OSA is weighted by its amount of solar  
334 energy under the standard solar spectra ASTM E-490 AM0 (Shanmugam and Ahn, 2007),  
335  $E(\lambda)$  assumption as follows.

336 
$$OSA(\theta, w, Chl) = \int_{\lambda_1=200}^{\lambda_2=4000} E(\lambda) OSA(\lambda, \theta, w, Chl) d\lambda \bigg/ \int_{\lambda_1=200}^{\lambda_2=4000} E(\lambda) d\lambda$$

337

338 Tabulated values for  $E(\lambda)$  are given in Table S1.

339 Finally for the total incoming radiation, the OSA can be written as:

340  $OSA(\theta, w, Chl) = (F_{dir} OSA_{dir}(\theta, w, Chl) + F_{dif} OSA_{dif}(\theta, w, Chl)) / (F_{dir} + F_{dif})$

341 where  $F_{dir}$  and  $F_{dif}$  are the downward surface fluxes of direct and diffuse radiation,  
342 respectively.  $OSA(\theta, w, Chl)$  is then computed for each model ocean grid cell at each model  
343 time-step. it should be noted that the SZA used in LMDZ is the average of the SZA during the  
344 daytime fraction of the time step.

351

### 352 3 Contribution of various OSA components

353 In this section, we analyze the geographical structure of OSA which is decomposed as  
354 follows:

$$355 \quad A_{dir}(\theta, w, Chl) = \int_{\lambda_1=200}^{\lambda_2=4000} E(\lambda)(\alpha_{dir}^S(\lambda, \theta, w) + \alpha_{dir}^W(\lambda, \theta, Chl)) d\lambda \bigg/ \int_{\lambda_1=200}^{\lambda_2=4000} E(\lambda) d\lambda$$

$$356 \quad A_{dif}(\theta, w, Chl) = \int_{\lambda_1=200}^{\lambda_2=4000} E(\lambda)(\alpha_{dif}^S(\lambda, \theta, w) + \alpha_{dif}^W(\lambda, Chl)) d\lambda \bigg/ \int_{\lambda_1=200}^{\lambda_2=4000} E(\lambda) d\lambda$$

$$357 \quad A_{wc} = \int_{\lambda_1=200}^{\lambda_2=4000} E(\lambda)\alpha^{WC}(\lambda) d\lambda \bigg/ \int_{\lambda_1=200}^{\lambda_2=4000} E(\lambda) d\lambda = 0.174$$

358

359 where  $A_{dir}$  and  $A_{dif}$  are the broadband ocean surface albedos for direct and diffuse radiation  
360 in the absence of whitecaps albedo; and  $A_{wc}$  is the broadband albedo of whitecaps.

361  $A_{dir}$ ,  $A_{dif}$  and  $A_{wc}$  have been estimated from offline calculations using Era-Interim forcing  
362 fields from 2000 to 2009 at monthly frequency (Dee et al., 2011) and chlorophyll climatology  
363 from SeaWiFS (Siegel et al., 2002). Compared to  $A_{dir}$  and  $A_{dif}$ ,  $A_{wc}$  is constant in space;  
364 therefore its geographical structure arises from whitecaps coverage (WC).

365

366 Figure 3a show that  $A_{dir}$  displays a strong meridional gradient with high values over high  
367 latitude oceans and low values over the tropical oceans. It confirms that the solar zenith angle  
368 is the prominent drivers of  $A_{dir}$ . This albedo exhibits nonetheless geographical structure over  
369 the tropical oceans which are linked to the easterlies wind regimes which suggest that surface  
370 winds variability may imprint a small but noticeable influence on the ocean surface albedo for  
371 direct radiation.

372

373 Compared to  $A_{dir}$ ,  $A_{dif}$  does not exhibit such a large meridional gradient (Figures 3b).  $A_{dif}$   
374 shows values close to 0.06. It displays nonetheless values  $> 0.06$  over the subtropical gyres  
375 and values  $< 6\%$  over the North Atlantic and the Southern Ocean in response to the 10 m  
376 wind speeds. Those patterns are related to surface winds pattern but also to the geographical  
377 structure of oligotrophic gyres with low chlorophyll values which reinforce the contribution  
378 of the ocean interior reflectance to surface albedo for the diffuse incoming radiation.

Supprimé:  $\alpha_{wc}$

Supprimé: enhancing

Supprimé: below-water

Supprimé: of

383

384 Figures 3c provides further insight on the regional influence of WC which display a  
385 broadband albedo of 0.174. Offline calculation of WC shows that whitecaps influence albedo  
386 for direct and diffuse radiation where westerly winds blow regularly, that is ~~e.g.,~~ in the  
387 Southern Ocean, the North Atlantic and the North Pacific. A weaker but noticeable influence  
388 is also found over the tropical oceans.

389 While  $A_{wc}$  is larger than  $A_{dir}$  and  $A_{dif}$ , the convolution of broadband albedo of the whitecaps  
390 and their coverage results in maximal contribution of 0.003 to the broadband albedos for  
391 direct and diffuse radiation. Yet, its strong albedo makes the whitecaps an important player at  
392 interannual and climate timescales. Indeed, this component of OSA for direct and diffuse  
393 radiation is subject to respond to the interannual variability of 10 m wind speed and also to  
394 climate change. Indeed, the contraction of Southern Ocean westerly winds (e.g., Boening et  
395 al., 2008) might induce subtle regional fluctuations in OSA that can feedback on the climate  
396 response.

397

398

## 399 **4 Materials and methods**

### 400 **4-1 Observations**

401 To assess model reliability to simulate realistic OSA, we compare fields to available  
402 observations. For those observations, we estimate the time-averaged OSA from the ratio  
403 between the time-averaged upwelling and downwelling shortwave radiative fluxes provided  
404 in those datasets.

405

406 At local scale, we use the CERES Ocean Validation Experiment (COVE, (Rutledge et al.,  
407 2006)) ground-based measurements. This instrument ocean platform located at Chesapeake  
408 bay provides continuous measurements of several radiative fluxes since 2001. In this study,  
409 we use measurements of upwelling and downwelling global (i.e., direct and diffuse)  
410 shortwave radiation averaged across several instruments  
411 (<https://cove.larc.nasa.gov/instruments.html>).

412

413 At global scale, we perform model evaluation with retrievals from the CERES satellite  
414 radiation measurements (Wielicki et al., 1996). CERES data provides estimates of global  
415 shortwave radiation at top of the atmosphere and at the surface. In the present study, we focus

Supprimé: i.e.

417 on surface estimates since our analyses aims at assessing the representation of ocean surface  
418 albedo.

419  
420

## 421 **4-2 Models**

### 422 **4-2-1 LMDZ v5A**

423 LMDZ is an atmospheric general circulation model developed at the Laboratoire de  
424 Météorologie Dynamique. The version of this atmosphere model, so-called LMDZ\_v5A, is  
425 described in detail in Hourdin et al. (2013) ; it is part of the main IPSL climate model used for  
426 CMIP5 and described in Dufresne et al. (2013) (IPSL-CM5A). The atmospheric resolution is  
427 96x95 on the horizontal and 39 layers on the vertical. The old OSA scheme in this version of  
428 LMDZ is based on the formulation of Larsen and Barkstrom (1977). It is parameterized in  
429 terms of  $\mu$  as follows:

$$430 \alpha_{dir}^S(\theta) = \frac{0.058}{\mu + 0.30}$$

431 Consequently, OSA varies between 0.0446 for a sun at zenith and 0.193 for a sun at the  
432 horizon. Direct and diffuse radiation are not distinguished and only a broadband albedo is  
433 used in the visible spectrum ( $\alpha_{dif}^S = \alpha_{dir}^S$ ).

434 In LMDZ, the partitioning between direct and diffuse light is derived from the presence of  
435 cloud in the atmosphere model grid-cell.

436

437 We assess simulated OSA using an atmosphere-only simulation with prescribed radiative  
438 forcing (greenhouse gases, aerosols, land-cover change) and fixed sea-surface temperature as  
439 recommended by CMIP5 (Taylor et al., 2011). LMDZ has been integrated from 1979 up to  
440 2012 under this protocol.

441 Similarly to the observations, simulated OSA at a given frequency is derived from ratio  
442 between the time-averaged upwelling and downwelling shortwave radiative fluxes at that  
443 frequency.

444

### 445 **4-2-2 ARPEGE-Climat v6.1**

446 ARPEGE-Climat v6.1 derives from ARPEGE-Integrated Forecasting System (IFS), the  
447 operational numerical weather forecast models of Météo-France and the European Centre for  
448 Medium-Range Weather Forecasts (ECMWF). Compared to version used in (Voldoire et al.,  
449 2013), several improvements in atmospheric physics have been implemented. They consist in

Mis en forme: Police :Gras

450 a new vertical diffusion scheme which solves a prognostic turbulent kinetic energy equation  
451 following Cuxart et al. (2000), an updated prognostic microphysics representing the specific  
452 masses of cloud liquid and ice water, rain and snow, as detailed in Lopez (2002), and a new  
453 convection scheme known as the Prognostic Condensates Microphysics Transport PCMT  
454 (Gu er emy, 2011; Piriou et al., 2007). ARPEGE-Climat v6.1 is implicitly coupled to the  
455 surface model called SURFEX (Masson et al., 2013), which considers a diversity of surface  
456 formulations for the evolution of four types of surface: land, town, inland water and ocean.  
457 The old OSA formulation implemented in SURFEX follows Taylor et al. (1996). This scheme  
458 enables the computation of  $\alpha_{dir}^S$  as a function of  $\mu$ :

$$459 \alpha_{dir}^S(\theta) = \frac{0.037}{1.1\mu^{1.4} + 0.15}$$

460 Since this schema does not enable computation of  $\alpha_{dif}^S$ ,  $\alpha_{dif}^S$  is set to a constant value of  
461 0.066.

462 Like LMDZ, the partitioning of direct and diffuse radiation depends on the cloud cover in the  
463 atmospheric model grid-cell.

464

465 Simulations performed with ARPEGE-Climat also consists in an AMIP simulations as  
466 LMDZ, except for sea-surface temperature which relies on data recommended by CMIP6  
467 (Eyring et al., 2016a). This simulation also spans from 1979 up to 2012.

468 Analyses are complemented using another simulation of ARPEGE-Climat in which the  
469 resolved dynamics is nudged towards that of Era-Interim. Nudging consists in restoring the  
470 model wind divergence and vorticity and the surface pressure towards those from Era-Interim.

471 The restoring timescale is 12 hours for the wind divergence and surface pressure and 6 hours  
472 for the wind vorticity. This simulation is employed hereafter as a kind of reference of what  
473 could be expected by the OSA parameterization if the wind spatio-temporal properties were  
474 “realistic”. In this case, only the direct-to-diffuse incident radiation partitioning remains tied  
475 to ARPEGE-Climat. This simulation replicates the chronology of the observed day-to-day  
476 variability of 10m wind speed and hence is expected to be closer to the ground-based  
477 observations.

478 For those models simulations, simulated OSA at a given frequency is diagnosed from ratio  
479 between the time-averaged upwelling and downwelling shortwave radiative fluxes at that  
480 frequency.

481

482

483 **5 Comparison of analytical calculation**

484 In order to better understand changes in simulated OSA, we compare first analytical solution  
485 of old and new interactive OSA schemes used in the two atmospheric models for both direct  
486 and diffuse radiation (Figure 4). We also compare old and new interactive OSA schemes to  
487 Payne (1972) OSA scheme that is currently used in numbers of atmospheric and ocean  
488 models such as NEMO (Madec, 2008).

489 Figure 4a shows that old OSA schemes for direct radiation differ in term of response to solar  
490 zenith angle. Indeed, for a given solar zenith angle, the scheme used in LMDZ (Larsen and  
491 Barkstrom, 1977) leads to a greater OSA than that used in ARPEGE-Climat (Taylor et al.,  
492 1996). The shape of the response to variations in solar zenith angle suggests that the scheme  
493 used in ARPEGE-Climat leads to a slightly stronger meridional gradient in OSA than that  
494 used in LMDZ. Interestingly, the new scheme produces OSA values bracketed by those of old  
495 algorithms, except for small solar zenith angle. Under this condition, the effect of winds is to  
496 increase OSA up to 0.072. It also displays a greater response to variations in solar zenith  
497 angle which differs substantially from those given by the old schemes.

498 Compared to Payne (1972) OSA scheme old and new schemes used in the two atmosphere  
499 models exhibit a weaker meridional gradient in OSA (Figure 4a). However, the meridional  
500 gradient as estimated by Payne (1972) is similar to that produced by Taylor et al. (1996)  
501 because their formulations solely differ by a coefficient: that is 0.037 for Taylor et al. (1996),  
502 0.05 for Payne (1972).

503  
504 Differences in OSA for diffuse radiation presented in Figure 4b are noticeable. They clearly  
505 illustrate modelling assumptions in the old schemes. Indeed, old schemes have been built on  
506 *ad hoc* formulations. Neither Taylor et al. (1996) nor Larsen and Barkstrom (1977) have  
507 provided a differentiated OSA for direct and diffuse radiation. This is why OSA for diffuse  
508 radiation is set to 0.06 (corresponding to the angular average of the OSA for direct radiation)  
509 in ARPEGE-Climat, whereas that of LMDZ is equal to the OSA for direct radiation from  
510 Larsen and Barkstrom (1977).

511 Figure 4b shows that the new interactive scheme displays feature similar to the diffuse OSA  
512 used in ARPEGE-Climat or that estimated from Payne (1972). This scheme produces  
513 nonetheless slightly larger values which can fluctuate in response to other drivers. The old  
514 OSA for diffuse radiation employed in LMDZ responds to variations in solar zenith angle  
515 while it should not. Errors related to this erroneous representation of OSA for diffuse  
516 radiation is also modulated by the partitioning between direct and diffuse radiation estimated

Supprimé: .

Supprimé: .

519 by the atmospheric model.

520

## 521 **6 Evaluation at COVE station (36.905°N, 75.713°W)**

522 In this section, we employ COVE daily data to assess the simulated OSA by both atmospheric  
523 models at local scale. OSA is computed here as the ratio of averaged radiation fluxes at daily  
524 resolution for both ground-based observations and models. Such an evaluation is fundamental  
525 because it relies on direct ground-truth observations over the ocean surface and hence  
526 provides a more accurate assessment of the OSA scheme as compared to the global-scale  
527 satellite-derived estimates developed in the following sections.

528

529 Figure 5 shows how well model using old and new interactive OSA scheme behaves at daily  
530 frequency compared to the ground-based observations at COVE station from 2001 to 2009.  
531 Figure 5 and Figure S1a clearly shows that both old OSA schemes of ARPEGE-Climat or  
532 LMDZ fail at replicating day-to-day OSA variations at the COVE station. Comparatively,  
533 Figure 5 and Figure S1b emphasizes how much the new interactive scheme improves OSA as  
534 simulated by both atmospheric models. Indeed, the simulated OSA are now consistent with  
535 observation at COVE station, with temporal correlation greater than 0.3. However, the models  
536 fail at replicating the large OSA values occurring during the winter in ground-based  
537 observations.

538

539 Those findings are reinforced when we compare the probability density function (pdf)  
540 estimated from daily-mean OSA as simulated by models against that derived from ground-  
541 based observations (Figure 6). This analysis provides further insight on how old and new  
542 interactive OSA schemes behave at COVE station. Figure 6 confirms that old schemes fail at  
543 capturing the day-to-day variations in OSA. Indeed, day-to-day variations in OSA estimated  
544 from old schemes arise from day-to-day variations in SZA and to a lesser extent to variations  
545 in direct-to-diffuse ratio of incident radiation which are related to the cloud cover. As shown  
546 in Figure 4, old OSA schemes crudely represent diffuse albedo. Therefore, errors in direct-to-  
547 diffuse ratio of incident radiation imprint errors in the simulated OSA. Consequently, day-to-  
548 day variations are better reproduced when the albedo for diffuse radiation is realistically  
549 simulated (Figure 6). In particular, the new interactive scheme captures the minimum OSA  
550 values occurring during the summer which are lower than 0.06.

551

552

553 At seasonal scale, OSA estimated from averaged radiative fluxes agrees with the above-  
554 mentioned findings for ground-based observations and models. Figure 7 clearly shows that  
555 old OSA schemes do not capture seasonal variations of observed OSA. Correlation between  
556 observation-derived OSA and that simulated by both models is 0.32 for ARPEGE-Climat and  
557 0.28 for LMDZ, which is very low, indicating an unrealistic representation of OSA.  
558 Comparison with CMIP5 atmosphere models shows that OSA as simulated by ARPEGE-  
559 Climat or LMDZ are in the range of CMIP5 models (0.04–0.17), confirming the large  
560 uncertainties related to simulated OSA in state-of-the-art climate model. While several  
561 CMIP5 models replicate seasonal variation in OSA, most of them exhibit large biases in  
562 simulated OSA compared to the observation-based estimate. Only ACCESS1-3, BNU-ESM,  
563 HadCM3, MIROC-ESM and MIROC-ESM-CHEM display a mean seasonal cycle of OSA  
564 comparable to the observation-based estimate at COVE station. For ARPEGE-Climat, this  
565 erroneous representation of OSA at seasonal scale leads, at least for this location, to a  
566 systematic bias in the surface energy budget of +3 W m<sup>-2</sup> in winter and -1.5 W m<sup>-2</sup> in summer.  
567 It is thus likely that large deviation in OSA as simulated by CMIP5 lead to substantial errors  
568 in energy flow at the air-sea interface.

569 Figure 7 shows significant improvements in the simulated OSA in both models using the new  
570 interactive scheme. In both models, the simulated seasonal cycle of OSA replicates the  
571 minimum observed during the summer. Although using the new interactive OSA scheme,  
572 both models do not capture large values of OSA of 0.10 occurring during the winter. That  
573 said, model-data comparison shows that correlation with observations has been improved.  
574 Indeed, correlation between observed and simulated daily values over a mean yearly cycle has  
575 increased from 0.23 to 0.84 in LMDZ to 0.32 to 0.86 in ARPEGE-Climat.

577 Although improved, Figures 5, 6 and 7 show that new interactive OSA scheme seems to  
578 suffer from a systematic bias in winter and miss OSA values greater than 0.10. This is  
579 supported by the fact that this systematic bias is displayed for all model estimates  
580 independently from the atmospheric physics and dynamics (i.e., LMDZ, ARPEGE-Climat and  
581 nudged OSA). That being said, some other possible reasons can explain such deviations  
582 between models and ground-based data. First, current atmosphere models suffer from  
583 systematic errors in the ratio of direct-to-diffuse radiation which can be related to bias in  
584 cloud cover or aerosol optical thickness (as shown in Figure S2). A larger-than-observed  
585 atmospheric optical depth in winter may favor diffuse path with the respect to the direct path,  
586 resulting in a lower-than-observed OSA Second, coarse resolution atmospheric models are not

Mis en forme: p1

Supprimé: demonstrates

Supprimé: are unable to

Mis en forme: Police :12 pt, Couleur de police : Texte 1

Mis en forme: Police :12 pt, Couleur de police : Texte 1

Mis en forme: Police :12 pt, Couleur de police : Texte 1

Supprimé: T

Supprimé: However,

Supprimé: .



592 able to replicate the mesoscale meteorological and oceanic conditions at this very location.  
593 Differences in surface wind between the models and field conditions can increase the  
594 contribution of whitecaps albedo with the respect to that of the Fresnel reflectance. Third,  
595 local ocean conditions and the presence of ocean waves resulting from remoted wind  
596 influence (i.e., swell) are not simulated by the atmospheric models. This would lead to an  
597 underestimate of the contributions of both whitecaps and Fresnel reflectance.

598

## 599 **7 Global-scale evaluation**

### 600 **7-1 Climatological mean**

601 This section is dedicated to evaluate OSA at global-scale using global satellite product that  
602 are routinely used in Earth system models evaluation (Eyring et al., 2016b; Gleckler et al.,  
603 2008). We thus use OSA retrieved from CERES surface product to assess the simulated OSA  
604 by ARPEGE-Climat and LMDZ.

605 Figure 8 presents geographical pattern of OSA as simulated by ARPEGE-Climat and LMDZ  
606 using Taylor et al. (1996) and Larsen and Barkstrom (1977) schemes, respectively. These old  
607 OSA schemes were used during CMIP5 and thus give an idea of errors in the models'  
608 radiative budgets.

609 Globally, the simulated OSA overestimates the CERES-derived estimate ( $\sim 0.058$ ) by about  
610  $0.007$ . Yet, the most striking feature is the substantial differences in the meridional structure.  
611 CERES-derived OSA shows maximum values over the high-latitudes oceans and minimum  
612 values over the tropical oceans. None of the models using old schemes are able to capture this  
613 meridional structure. Deviations are particularly high for LMDZ, which hardly replicates  
614 maximum OSA over high-latitude oceans and minimum OSA over tropical oceans. Both  
615 models exhibit poor spatial correlation with  $-0.03$  for LMDZ and  $0.40$  for ARPEGE-Climat.  
616 Model-data errors in OSA mirror model bias in surface upwelling shortwave radiation, which  
617 amounts to  $\sim 7 \text{ W m}^{-2}$  over the tropical oceans compared to CERES.

618 The new interactive scheme improves favorably the comparison with observations (Figure 8).  
619 Indeed global mean OSA is equal to  $0.062$  for LMDZ and  $0.057$  for ARPEGE-Climat, which  
620 better matches the value derived from CERES data. As such, the model bias in surface  
621 upwelling shortwave radiation has been reduced by  $\sim 1 \text{ W m}^{-2}$  in average over the ocean and  
622 by up to  $\sim 5 \text{ W m}^{-2}$  over the tropical oceans.

623 Both models capture the meridional structure of the OSA with spatial correlations of about  
624  $0.82$  for LMDZ and  $0.86$  for ARPEGE-Climat. Nonetheless, the simulated OSA displays  
625 some biases. In LMDZ and ARPEGE-Climat, the modeled OSA over the North Atlantic is

626 slightly overestimated and shifted to the South. Major differences between simulated OSA are  
627 noticeable over the tropical oceans, where models differ in terms of zonal structure. LMDZ  
628 displays OSA of  $\sim 0.06$  over Eastern boundary upwelling systems, which is slightly too high  
629 compared to CERES. Differences in the OSA geographical structure between ARPEGE-  
630 Climat and LMDZ arise from differences in 10-meter wind speed (Figure S3) and direct-to-  
631 diffuse incident radiation as diagnosed from the simulated cloud cover (Figure S4). Large-  
632 scale deviations between models and observations seem to be related to differences in 10-  
633 meter wind fields (Figure S3). Model-data deviations in OSA at the regional scale rather  
634 mirror biases in total cloud cover (Figure S4). This is especially clear over low-latitude oceans  
635 where LMDZ overestimate OSA over the eastern boundary upwelling systems where LMDZ  
636 overestimates the cloud cover (Figure S4). This result is expected since over the low-latitude  
637 oceans the contribution of diffuse OSA is stronger than that of direct OSA (Figures 3 and 4).

638

### 639 **7-2 Seasonal variability**

640 Figure 9 compares the simulated and CERES-derived OSA on the seasonal scale. This time  
641 scale matters for modelling accurately the Earth's climate because the flow of incoming  
642 radiation fluctuates up to one order of magnitude between winter and summer at high  
643 latitudes.

644 Figure 9abc shows that both models using old OSA schemes hardly reproduce the seasonal  
645 cycle of OSA derived from CERES. This is particularly the case for LMDZ, which produced  
646 an unrealistic seasonal cycle for OSA. LMDZ fails at simulating maximum OSA during the  
647 winter of both hemispheres. Instead, extreme values of simulated OSA occur at  $50^{\circ}\text{N}$  and  
648  $50^{\circ}\text{S}$  during the summer. Simulated OSA in ARPEGE-Climat does not present these features  
649 but is biased high at all seasons.

650 With the new interactive scheme, the seasonal OSA is improved in both models (Figure 9de).  
651 The simulated OSA matches that derived from CERES at seasonal scale, with high values  
652 during the winter and low values between  $30^{\circ}\text{S}$  and  $30^{\circ}\text{N}$ . Improvement is especially  
653 noticeable for LMDZ which captures the observed seasonal cycle of OSA.

654 However, a few errors remain in the simulated OSA. In LMDZ, OSA is slightly too high  
655 compared to CERES ( $\sim 0.002$ ) in boreal and austral summer. Nonetheless, simulated OSA  
656 reproduces realistic OSA values in the tropics ( $\sim 5.2\%$ ). In ARPEGE-Climat, instead, the  
657 simulated OSA seems slightly too low compared to CERES ( $\sim 0.002$ ). This leads ARPEGE-  
658 Climat to overestimate the fraction of low-OSA ocean. Interestingly this bias solely concerns  
659 the tropical oceans. Indeed, simulated OSA over high-latitude oceans displays realistic

660 features at the seasonal scale. The fact that errors in ARPEGE-Climat and LMDZ are of  
661 different signs tends to suggest that the new interactive scheme is not intrinsically biased. It  
662 rather points to biases in driving fields such as the surface wind speeds or the ratio between  
663 direct and diffuse shortwave radiation simulated by either ARPEGE-Climat or LMDZ (Figure  
664 S2).

665  
666

## 667 8- Conclusions

668 In this paper, we have detailed a new interactive scheme for ocean surface albedo suited for  
669 Earth system models. This scheme computes the ocean surface albedo accounting for the  
670 spectral dependence (across a range of wavelengths between 200 and 4000 nm), the  
671 characteristics of incident solar radiation (direct or diffuse), the effects of surface winds,  
672 chlorophyll content and whitecaps in addition to the canonical solar zenith angle dependence.

673 This scheme enables an improved air-sea exchange of solar radiation. It thus provides a much  
674 more physical basis to resolve the radiative transfer at the interface between the atmosphere  
675 and the upper ocean and offer a suite of processes that are included in complex stand-alone  
676 ocean radiative transfer software such as HYDROLIGHT (Ohlman, Siegel and Mobley,  
677 2000). This work can be extended to include a coupling to an ocean wave model that would  
678 provide a more realistic distribution of ocean surface state.

Supprimé:  
Supprimé: a better coupling between the atmospheric and oceanic components of the model

679  
680 Although direct and diffuse albedos were included in the old ocean albedo schemes of the two  
681 atmospheric models used here, our results demonstrate that their assumptions employed for  
682 diffuse albedo (i.e., fixed values or equal to the direct albedo) are not realistic. The new  
683 interactive scheme improves its representation which leads to substantially reduce model-data  
684 error in ocean surface albedo over the low-latitude oceans.

Supprimé: .

Supprimé:

685  
686 Comparison to available dataset shows, for at least two state-of-the-art climate models, a  
687 noticeable improvement in terms of simulated ocean surface albedo compared to their old  
688 ocean surface albedo schemes. At the global scale, geographical pattern of simulated ocean  
689 surface albedo has been improved in both models. The simulated seasonal cycle also shows a  
690 noticeable improvement, especially in LMDZ, with a better correlation to CERES data (up to  
691 0.8). At the local scale, simulated ocean surface albedo also fits ocean surface albedo derived  
692 from ground-based radiative measurements at daily resolution with an improved correlation  
693 up to 0.8.

699

700 Compared to old schemes, the new interactive scheme is more complex and induces a small  
701 increase in model elapsed time of about 0.2%. Although noticeable, this increase does not  
702 preclude centennial-long simulation or high resolution model simulations.

Supprimé: slight

703

704 Improved ocean surface albedo might lead to difference in the simulated climate or marine  
705 biogeochemistry dynamics which will be assessed in future work. Indeed, a difference of  
706 about 1% of simulated ocean surface albedo for a global mean irradiance of  $\sim 180 \text{ W m}^{-2}$  can  
707 induce a deviation in energy flow of the Earth system comparable to the impact of land-cover  
708 changes over land (Myhre et al., 2013).

709

710

#### 711 **Code availability:**

712 The interactive ocean surface albedo code detailed in the paper is a part of the SURFEX  
713 (V8.0) ocean scheme and is available as open source via [http://www.cnrm-game-](http://www.cnrm-game-meteo.fr/surfex/)  
714 [meteo.fr/surfex/](http://www.cnrm-game-meteo.fr/surfex/). SURFEX (V8.0) is updated at a relatively low frequency (every 3 to 6  
715 months) and the developments presented in this paper are available starting from SURFEX  
716 (V8.0). If more frequent updates are needed, or if what is required is not in Open-SURFEX  
717 (DrHOOK, FA/LFI formats, GAUSSIAN grid), you are invited to follow the procedure to get  
718 a SVN account and to access real-time modifications of the code (see the instructions at the  
719 previous link. Besides, all the tabulated values use for this algorithm are available in the  
720 supplementary materials.

Supprimé: version 8.0

Mis en forme: Police :Times, 12 pt, Anglais (E.U.)

Mis en forme: Anglais (E.U.)

Supprimé: a

Mis en forme: Police :Times, 12 pt, Anglais (E.U.)

Supprimé: The LMDZ implementation is available as part of the LMDZ code which can be downloaded at <http://LMDZ.lmd.jussieu.fr/>.

Mis en forme: Police par défaut, Police :Times New Roman, Français

Supprimé: .

721

#### 722 *Acknowledgement:*

723 *This work was supported by the H2020 project CRESCENDO “Coordinated Research in*  
724 *Earth Systems and Climate : Experiments, kNowledge, Dissemination and Outreach” which*  
725 *received funding from the European Union’s Horizon 2020 research and innovation*  
726 *programme under grant agreement No 641816, the Labex L-IPSL which is funded by the ANR*  
727 *(Grant #ANR-10-LABX-0018) and by the European FP7 IS-ENES2 project (Grant #312979)”.  
728 The LMDZ simulations in this work were performed using TGCC resources under the GENCI*  
729 *(Grand Equipement National de Calcul Intensif) computer time allocation (grant 2016-*  
730 *t2014012201).*

731

740 **References:**

- 741 Allen, M. R., Frame, D. J., Huntingford, C., Jones, C. D., Lowe, J. A., Meinshausen, M. and  
742 Meinshausen, N.: Warming caused by cumulative carbon emissions towards the trillionth  
743 tonne, *Nature*, 458(7242), 1163–1166, doi:10.1038/nature08019, 2009.
- 744 Aouf, L., Lefevre, J.-M. and Hauser, D.: Assimilation of Directional Wave Spectra in the  
745 Wave Model WAM: An Impact Study from Synthetic Observations in Preparation for the  
746 SWIMSAT Satellite Mission, *J. Atmos. Oceanic Technol.*, 23(3), 448–463,  
747 doi:10.1175/JTECH1861.1, 2006.
- 748 Ardhuin, F., Rogers, E., Babanin, A. V., Filipot, J.-F., Magne, R., Roland, A., van der  
749 Westhuysen, A., Queffelec, P., Lefevre, J.-M., Aouf, L. and Collard, F.: Semiempirical  
750 Dissipation Source Functions for Ocean Waves. Part I: Definition, Calibration, and  
751 Validation, *J. Phys. Oceanogr.*, 40(9), 1917–1941, doi:10.1175/2010JPO4324.1, 2010.
- 752 Behrenfeld, M. J. and Falkowski, P. G.: Photosynthetic rates derived from satellite-based  
753 chlorophyll concentration, *Limnology and Oceanography*, 42(1), 1–20 [online] Available  
754 from: [http://www.es.ucsc.edu/~rkudela/OS130/OS130\\_1116A.PDF](http://www.es.ucsc.edu/~rkudela/OS130/OS130_1116A.PDF), 1997.
- 755 Behrenfeld, M. J., Randerson, J. T., McClain, C. R., Feldman, G. C., Los, S. O., Tucker, C. J.,  
756 Falkowski, P. G., Field, C. B., Frouin, R., Esaias, W. E., Kolber, D. D. and Pollack, N. H.:  
757 Biospheric Primary Production During an ENSO Transition, *Science*, 291(5513), 2594–2597,  
758 doi:10.1126/science.1055071, 2001.
- 759 Bell, T. G., De Bruyn, W., Miller, S. D., Ward, B., Christensen, K. and Saltzman, E. S.: Air-  
760 sea dimethylsulfide (DMS) gas transfer in the North Atlantic: evidence for limited interfacial  
761 gas exchange at high wind speed, *Atmos. Chem. Phys.*, 13(21), 11073–11087,  
762 doi:10.5194/acp-13-11073-2013, 2013.
- 763 Böning, C. W., Disper, A., Visbeck, M., Rintoul, S. R. and Schwarzkopf, F. U.: The response  
764 of the Antarctic Circumpolar Current to recent climate change, *Nature Geoscience*, 1(12),  
765 864–869, doi:10.1038/ngeo362, 2008.
- 766  
767 Chandrasekhar, S.: Radiative heat transfer, Dover Publications, New York, 11, 11–12, 1960.
- 768 Chepfer, H., Bony, S., Winker, D., Cesana, G., Dufresne, J.-L., Minnis, P., Stubenrauch, C. J.  
769 and Zeng, S.: The GCM-Oriented CALIPSO Cloud Product (CALIPSO-GOCCP), *J.*  
770 *Geophys. Res.*, 15, D00H16, doi:10.1029/2009JD012251, 2010.
- 771  
772 Clough, S. A., Shephard, M. W., Mlawer, E. J., Delamere, J. S., Iacono, M. J., Cady-Pereira,  
773 K., Boukabara, S. and Brown, P. D.: Atmospheric radiative transfer modeling: a summary of  
774 the AER codes, *Journal of Quantitative Spectroscopy and Radiative Transfer*, 91(2), 233–244,  
775 2005.
- 776 Cox, C. and Munk, W.: Measurement of the Roughness of the Sea Surface from Photographs  
777 of the Sun's Glitter, *J. Opt. Soc. Am.*, 44(11), 838–850, 1954.
- 778 Cuxart, J., Bougeault, P. and Redelsperger, J. L.: A turbulence scheme allowing for mesoscale  
779 and large-eddy simulations, *Q.J.R. Meteorol. Soc.*, 126(562), 1–30,

780 doi:10.1002/qj.49712656202, 2000.

781 Deane, G. B. and Stokes, M. D.: Scale dependence of bubble creation mechanisms in  
782 breaking waves, *Nature*, 418(6900), 839–844, doi:10.1038/nature00967, 2002.

783 Dee, D. P., Uppala, S. M., Simmons, A. J., Berrisford, P., Poli, P., Kobayashi, S., Andrae, U.,  
784 Balmaseda, M. A., Balsamo, G., Bauer, P., Bechtold, P., Beljaars, A. C. M., van de Berg, L.,  
785 Bidlot, J., Bormann, N., Delsol, C., Dragani, R., Fuentes, M., Geer, A. J., Haimberger, L.,  
786 Healy, S. B., Hersbach, H., Hólm, E. V., Isaksen, L., Kållberg, P., Köhler, M., Matricardi, M.,  
787 McNally, A. P., Monge-Sanz, B. M., Morcrette, J. J., Park, B. K., Peubey, C., de Rosnay, P.,  
788 Tavolato, C., Thépaut, J. N. and Vitart, F.: The ERA-Interim reanalysis: configuration and  
789 performance of the data assimilation system, *Q.J.R. Meteorol. Soc.*, 137(656), 553–597, 2011.

790 Dufresne, J.-L., Foujols, M. A., Denvil, S., Caubel, A., Marti, O., Aumont, O., Balkanski, Y.,  
791 Bekki, S., Bellenger, H., Benshila, R., Bony, S., Bopp, L., Braconnot, P., Brockmann, P.,  
792 Cadule, P., Cheruy, F., Codron, F., Cozic, A., Cugnet, D., Noblet, N., Duvel, J. P., Ethe, C.,  
793 Fairhead, L., Fichefet, T., Flavoni, S., Friedlingstein, P., Grandpeix, J. Y., Guez, L.,  
794 Guilyardi, E., Hauglustaine, D., Hourdin, F., Idelkadi, A., Ghattas, J., Joussaume, S.,  
795 Kageyama, M., Krinner, G., Labetoulle, S., Lahellec, A., Lefebvre, M.-P., Lefèvre, F., Lévy,  
796 C., Li, Z. X., Lloyd, J., Lott, F., Madec, G., Mancip, M., Marchand, M., Masson, S.,  
797 Meurdesoif, Y., Mignot, J., Musat, I., Parouty, S., Polcher, J., Rio, C., Schulz, M.,  
798 Swingedouw, D., Szopa, S., Talandier, C., Terray, P., Viovy, N. and Vuichard, N.: Climate  
799 change projections using the IPSL-CM5 Earth System Model: from CMIP3 to CMIP5, *Clim  
800 Dyn*, 40(9–10), 2123–2165, doi:10.1007/s00382-012-1636-1, 2013.

801 Dutkiewicz, S., Hickman, A. E., Jahn, O., Gregg, W. W., Mouw, C. B. and Follows, M. J.:  
802 Capturing optically important constituents and properties in a marine biogeochemical and  
803 ecosystem model, *Biogeosciences Discuss.*, 12(3), 2607–2695, doi:10.5194/bgd-12-2607-  
804 2015, 2015.

805 Eyring, V., Bony, S., Meehl, G. A., Senior, C. A., Stevens, B., Stouffer, R. J. and Taylor, K.  
806 E.: Overview of the Coupled Model Intercomparison Project Phase 6 (CMIP6) experimental  
807 design and organization, *Geosci. Model Dev*, 9(5), 1937–1958, doi:10.5194/gmd-9-1937-  
808 2016, 2016a.

809 Eyring, V., Gleckler, P. J., Heinze, C., Stouffer, R. J., Taylor, K. E., Balaji, V., Guilyardi, E.,  
810 Joussaume, S., Kindermann, S., Lawrence, B. N., Meehl, G. A., Righi, M. and Williams, D.  
811 N.: Towards improved and more routine Earth system model evaluation in CMIP, *Earth Syst.  
812 Dynam.*, 7(4), 813–830, doi:10.5194/esd-7-813-2016, 2016b.

813 Frigaard, N.-U., Larsen, K. L. and Cox, R. P. A.: Spectrochromatography of photosynthetic  
814 pigments as a fingerprinting technique for microbial phototrophs, *FEMS Microbiology  
815 Ecology*, 20(2), 69–77, doi:10.1111/j.1574-6941.1996.tb00306.x, 1996.

816 Frouin, R., Iacobellis, S. F. and Deschamps, P. Y.: Influence of oceanic whitecaps on the  
817 Global Radiation Budget, *Geophys. Res. Lett.*, 28(8), 1523–1526,  
818 doi:10.1029/2000GL012657, 2001.

819 Frouin, R., Schwindling, M. and Deschamps, P.-Y.: Spectral reflectance of sea foam in the  
820 visible and near-infrared: In situ measurements and remote sensing implications, *J. Geophys.  
821 Res.*, 101(C6), 14361–14371, doi:10.1029/96JC00629, 1996.

- 822 Frölicher, T. L.: Climate response: Strong warming at high emissions, *Nature Clim. Change*,  
823 6(9), 823–824, doi:10.1038/nclimate3053, 2016.
- 824 Gillett, N. P., Arora, V. K., Matthews, D. and Allen, M. R.: Constraining the Ratio of Global  
825 Warming to Cumulative CO<sub>2</sub> Emissions Using CMIP5 Simulations\*, *J. Climate*, 26(18),  
826 6844–6858, doi:10.1175/JCLI-D-12-00476.s1, 2013.
- 827 Gleckler, P. J., Taylor, K. E. and Doutriaux, C.: Performance metrics for climate models, *J.*  
828 *Geophys. Res.*, 113(D6), D06104, doi:10.1029/2007JD008972, 2008.
- 829 Gordon, H. R. and Wang, M.: Influence of oceanic whitecaps on atmospheric correction of  
830 ocean-color sensors, *Appl. Opt.*, 33(33), 7754–7763, doi:10.1364/AO.33.007754, 1994.
- 831 Guérémy, J. F.: A continuous buoyancy based convection scheme: one- and three-  
832 dimensional validation, *Tellus A*, 63(4), 687–706, doi:10.1111/j.1600-0870.2011.00521.x,  
833 2011.
- 834 Gupta, S., Ritchey, N., Wilber, A. and Whitlock, C.: A climatology of surface radiation  
835 budget derived from satellite data, *J. Climate*, 12, 2691–2710, [https://doi.org/10.1175/1520-](https://doi.org/10.1175/1520-0442(1999)012<2691:ACOSRB>2.0.CO;2)  
836 [0442\(1999\)012<2691:ACOSRB>2.0.CO;2](https://doi.org/10.1175/1520-0442(1999)012<2691:ACOSRB>2.0.CO;2), 1999.
- 837 Hansen, J., Russell, G., Rind, D., Stone, P., Lacis, A., Lebedeff, S., Ruedy, R. and Travis, L.:  
838 Efficient Three-Dimensional Global Models for Climate Studies: Models I and II, *Mon. Wea.*  
839 *Rev.*, 111(4), 609–662, doi:10.1175/1520-0493(1983)111<0609:ETDGMF>2.0.CO;2, 1983.
- 840
- 841 Hense, I., Stemmler, I. and Sonntag, S.: Ideas and perspectives: climate-relevant marine  
842 biologically driven mechanisms in Earth system models, *Biogeosciences*, 14(2), 403–413,  
843 doi:10.5194/bg-14-403-2017, 2017.
- 844 Hourdin, F., Foujols, M.-A., Codron, F., Guemas, V., Dufresne, J.-L., Bony, S., Denvil, S.,  
845 Guez, L., Lott, F., Ghattas, J., Braconnot, P., Marti, O., Meurdesoif, Y. and Bopp, L.: Impact  
846 of the LMDZ atmospheric grid configuration on the climate and sensitivity of the IPSL-  
847 CM5A coupled model, *Climate Dynamics*, 40(9-10), 2167–2192, doi:10.1007/s00382-012-  
848 1411-3, 2013.
- 849 IPCC, 2001: *Climate Change 2001: The Scientific Basis*, edited by T. J. Houghton, Y. Ding,  
850 D. J. Griggs, M. Noguer, P. J. van der Linden, X. Dai, K. Maskell, and C. A. Johnson,  
851 Cambridge University Press, Cambridge, United Kingdom and New York, NY, USA. 2001.
- 852 IPCC, 2007: *Climate Change 2007: The Physical Science Basis*, edited by S. Solomon, D.  
853 Qin, M. Manning, Z. Chen, M. Marquis, K. B. Averyt, M. Tignor, and H. L. Miller,  
854 Cambridge University Press, Cambridge, United Kingdom and New York, NY, USA. 2007.
- 855 IPCC, 2013: *Climate Change 2013: The Physical Science Basis.*, edited by T. F. Stoker, D.  
856 Qin, G. Plattner, M. Tignor, S. K. Allen, J. Boschung, A. Nauels, Y. Xia, V. Bex, and P. M.  
857 Midgley, Cambridge Univ Press, Cambridge, United Kingdom and New York, NY, USA.  
858 2013.
- 859 Irvine, W. M. and Pollack, J. B.: Infrared optical properties of water and ice spheres, *Icarus*,  
860 8(1), 324–360, 1968.
- 861 Jin, Z.: A parameterization of ocean surface albedo, *Geophys. Res. Lett.*, 31(22),

- 862 doi:10.1029/2004GL021180, 2004.
- 863 Jin, Z., Charlock, T. P. and Rutledge, K.: Analysis of Broadband Solar Radiation and Albedo  
864 over the Ocean Surface at COVE, *J. Atmos. Oceanic Technol.*, 19(10), 1585–1601,  
865 doi:10.1175/1520-0426(2002)019<1585:AOSBSRA>2.0.CO;2, 2002.
- 866 Jin, Z., Charlock, T. P., Rutledge, K., Cota, G., Kahn, R., Redemann, J., Zhang, T., Rutan, D.  
867 A. and Rose, F.: Radiative transfer modeling for the CLAMS experiment, *Journal of the*  
868 *atmospheric sciences*, 62(4), 1053–1071, 2005.
- 869 Jin, Z., Charlock, T. P., Rutledge, K., Stamnes, K. and Wang, Y.: Analytical solution of  
870 radiative transfer in the coupled atmosphere-ocean system with a rough surface, *Appl. Opt.*,  
871 45(28), 7443–7455, 2006.
- 872 Jin, Z., Qiao, Y., Wang, Y., Fang, Y. and Yi, W.: A new parameterization of spectral and  
873 broadband ocean surface albedo, *Optics Express*, 19(27), 26429–26443, 2011.
- 874 Kent, E. C., Forrester, T. N. and Taylor, P. K.: A comparison of oceanic skin effect  
875 parameterizations using shipborne radiometer data, *J. Geophys. Res.*, 101(C7), 16649,  
876 doi:10.1029/96JC01054, 1996.
- 877 Kim, G. E., Pradal, M. A. and Gnanadesikan, A.: A new parameterization for surface ocean  
878 light attenuation in Earth System Models: assessing the impact of light absorption by colored  
879 detrital material, *Biogeosciences Discuss.*, 12(5), 3905–3942, doi:10.5194/bgd-12-3905-2015,  
880 2015.
- 881 Koepke, P.: Effective reflectance of oceanic whitecaps, *Appl. Opt.*, 23(11), 1816–1824,  
882 doi:10.1364/AO.23.001816, 1984.
- 883 Larsen, J. C. and Barkstrom, B. R.: Effects of realistic angular reflection laws for the Earth's  
884 surface upon calculations of the Earth-atmosphere albedo, *Radiation in the Atmosphere*,  
885 *Proceedings of an International Symposium*, Princeton: Science Press, p. 451. 1977.  
886
- 887 Li, J., Scinocca, J., Lazare, M., McFarlane, N., Salzen, von, K. and Solheim, L.: Ocean  
888 Surface Albedo and Its Impact on Radiation Balance in Climate Models, *J. Climate*, 19(24),  
889 6314–6333, doi:10.1175/JCLI3973.1, 2006.
- 890 Li, T., Bai, Y., Li, G., He, X., Chen, C.-T., Gao, K. and Liu, D.: Effects of ultraviolet  
891 radiation on marine primary production with reference to satellite remote sensing, *Front.*  
892 *Earth Sci.*, 1–11, doi:10.1007/s11707-014-0477-0, 2014.
- 893 Lopez, P.: Implementation and validation of a new prognostic large-scale cloud and  
894 precipitation scheme for climate and data-assimilation purposes, *Q.J.R. Meteorol. Soc.*,  
895 128(579), 229–257, doi:10.1256/00359000260498879, 2002.
- 896 [Madec, G., Bissery, C., Crochelet, E., Meola, B., Webster, C., Claudet, J., ... Quod, C.](#)  
897 [\(2008\). \*NEMO ocean engine\*. \(Institut P\). \*Note du Pole de modélisation \(Vol. 27\)\*.](#)  
898 [Institut Pierre-Simon Laplace \(IPSL\). Retrieved from \[http://www.nemo-ocean.eu/About-\]\(http://www.nemo-ocean.eu/About-NEMO/Reference-manuals\)](#)  
899 [NEMO/Reference-manuals](#)
- 900 [Masson, V., Le Moigne, P., Martin, E., Faroux, S., Alias, A., Alkama, R., Belamari, S.,](#)

Supprimé: -



902 Barbu, A., Boone, A., Bouyssel, F., Brousseau, P., Brun, E., Calvet, J.-C., Carrer, D.,  
903 Decharme, B., Delire, C., Donier, S., Essaouini, K., Gibelin, A. L., Giordani, H., Habets, F.,  
904 Jidane, M., Kerdraon, G., Kourzeneva, E., Lafaysse, M., Lafont, S., Lebeaupin Brossier, C.,  
905 Lemonsu, A., Mahfouf, J. F., Marguinaud, P., Mokhtari, M., Morin, S., Pigeon, G., Salgado,  
906 R., Seity, Y., Taillefer, F., Tanguy, G., Tulet, P., Vincendon, B., Vionnet, V. and Voldoire,  
907 A.: The SURFEXv7.2 land and ocean surface platform for coupled or offline simulation of  
908 earth surface variables and fluxes, *Geosci. Model Dev*, 6(4), 929–960, doi:10.5194/gmd-6-  
909 929-2013-supplement, 2013.

910 Melville, W. K. and Matusov, P.: Distribution of breaking waves at the ocean surface, *Nature*,  
911 417(6884), 58–63, doi:10.1038/417058a, 2002.

912 Mlawer, E. J., Taubman, S. J., Brown, P. D., Iacono, M. J. and Clough, S. A.: Radiative  
913 transfer for inhomogeneous atmospheres: RRTM, a validated correlated-k model for the  
914 longwave, *J. Geophys. Res.*, 102(D14), 16663–16682, doi:10.1029/97JD00237, 1997.

915 Morel, A. and Antoine, D.: Heating rate within the upper ocean in relation to its bio-optical  
916 state, *J. Phys. Oceanogr.*, 24(7), 1652–1665, [https://doi.org/10.1175/1520-](https://doi.org/10.1175/1520-0485(1994)024<1652:HRWTUO>2.0.CO;2)  
917 [0485\(1994\)024<1652:HRWTUO>2.0.CO;2](https://doi.org/10.1175/1520-0485(1994)024<1652:HRWTUO>2.0.CO;2), 1994.  
918

919 Morel, A. and Gentili, B.: Diffuse reflectance of oceanic waters: its dependence on Sun angle  
920 as influenced by the molecular scattering contribution, *Appl. Opt.*, 30(30), 4427–4438,  
921 doi:10.1364/AO.30.004427, 1991.

922 Morel, A. and Maritorena, S.: Bio-optical properties of oceanic waters: A reappraisal, *Journal*  
923 *of Geophysical Research-Oceans*, 1 106(C4), 7163–7180, doi:10.1029/2000JC000319, 2001.  
924

925 Murtugudde, R., Beauchamp, J. and McClain, C. R.: Effects of penetrative radiation on the  
926 upper tropical ocean circulation, *J. Climate*, 15, 470–486, [https://doi.org/10.1175/1520-](https://doi.org/10.1175/1520-0442(2002)015<0470:EOPROT>2.0.CO;2)  
927 [0442\(2002\)015<0470:EOPROT>2.0.CO;2](https://doi.org/10.1175/1520-0442(2002)015<0470:EOPROT>2.0.CO;2), 2002.  
928

929 Myhre, G., Boucher, O., Breon, F.-M., Forster, P. and Shindell, D.: Declining uncertainty in  
930 transient climate response as CO2 forcing dominates future climate change, *Nature Geosci*,  
931 8(3), 181–185, doi:10.1038/ngeo2371, 2015.

932 Myhre, G., Shindell, D., Breon, F.-M., Collins, W., Fuglestedt, J., Huang, J., Koch, D.,  
933 Lamarque, J.-F., Lee, D., Mendoza, B., Nakajima, T., Robock, A., Stephens, G., Takemura, T.  
934 and Zhang, H.: Anthropogenic and Natural Radiative Forcing, *Climate Change 2013: The*  
935 *Physical Science Basis. Contribution of Working Group I to the Fifth Assessment Report of*  
936 *the Intergovernmental Panel on Climate Change*. 2013.

937 Nelson, D. M. and Smith, W. O. J.: The role of light and major nutrients, *Limnol. Oceanogr.*,  
938 36(8), 1650–1661, 1991.

939 Otto, A., Otto, F. E. L., Boucher, O., Church, J., Hegerl, G., Forster, P. M., Gillett, N. P.,  
940 Gregory, J., Johnson, G. C., Knutti, R., Lewis, N., Lohmann, U., Marotzke, J., Myhre, G.,  
941 Shindell, D., Stevens, B. and Allen, M. R.: Energy budget constraints on climate response, 6,  
942 415-416, doi:10.1038/ngeo1836, 2013.

- 943 Ohlmann, J. C., Siegel, D. A., & Mobley, C. D. (2000). Ocean Radiant Heating. Part I:  
 944 Optical Influences. *Journal of Physical Oceanography*, 30(8), 1833–1848.  
 945 [https://doi.org/10.1175/1520-0485\(2000\)030<1833:ORHPIO>2.0.CO;2](https://doi.org/10.1175/1520-0485(2000)030<1833:ORHPIO>2.0.CO;2)
- 946 Ohlmann, J. C., & Siegel, D. A. (2000). Ocean Radiant Heating. Part II: Parameterizing Solar  
 947 Radiation Transmission through the Upper Ocean. *Journal of Physical Oceanography*,  
 948 30(1996), 1849–1865. [https://doi.org/10.1175/1520-](https://doi.org/10.1175/1520-0485(2000)030<1849:ORHPIP>2.0.CO;2)  
 949 0485(2000)030<1849:ORHPIP>2.0.CO;2
- 950 Payne, R. E. (1972). Albedo of the Sea Surface. *Journal of the Atmospheric Sciences*, 29(5),  
 951 959–970. [https://doi.org/10.1175/1520-0469\(1972\)029<0959:AOTSS>2.0.CO;2](https://doi.org/10.1175/1520-0469(1972)029<0959:AOTSS>2.0.CO;2)
- 952 Piriou, J.-M., Redelsperger, J.-L., Geleyn, J.-F., Lafore, J.-P. and Guichard, F.: An Approach  
 953 for Convective Parameterization with Memory: Separating Microphysics and Transport in  
 954 Grid-Scale Equations, *J. Atmos. Sci.*, 64(11), 4127–4139, doi:10.1175/2007JAS2144.1, 2007.
- 955 Preisendorfer, R. W. and Mobley, C. D.: Albedos and Glitter Patterns of a Wind-Roughened  
 956 Sea Surface, *J. Phys. Oceanogr.*, 16(7), 1293–1316, doi:10.1175/1520-  
 957 0485(1986)016<1293:AAGPOA>2.0.CO;2, 1986.
- 958 Rutledge, C. K., Schuster, G. L., Charlock, T. P., Denn, F. M., Smith, W. L., Jr., Fabbri, B. E.,  
 959 Madigan, J. J., Jr. and Knapp, R. J.: Offshore Radiation Observations for Climate Research at  
 960 the CERES Ocean Validation Experiment: A New “Laboratory” for Retrieval Algorithm  
 961 Testing, *Bull. Amer. Meteor. Soc.*, 87(9), 1211–1222, doi:10.1175/BAMS-87-9-1211, 2006.
- 962 Salisbury, D. J., Anguelova, M. D. and Brooks, I. M.: Global Distribution and Seasonal  
 963 Dependence of Satellite-based Whitecap Fraction, *Geophys. Res. Lett.*, 2014GL059246,  
 964 doi:10.1002/2014GL059246, 2014.
- 965 Shanmugam, P. and Ahn, Y. H.: Reference solar irradiance spectra and consequences of their  
 966 disparities in remote sensing of the ocean colour, *Annales Geophysicae*, 25(6), 1235–1252,  
 967 doi:10.5194/angeo-25-1235-2007, 2007.
- 968 Siegel, D. A., Doney, S. C. and Yoder, J. A.: The North Atlantic spring phytoplankton bloom  
 969 and the Sverdrup's critical depth hypothesis, *Science*, 296, 730–733,  
 970 doi:10.1126/science.1069174, 2002.
- 971 Smith, E. D.: Water Characteristics, *Journal (Water Pollution Control Federation)*, 54(6),  
 972 541–554, 1982.
- 973 Smyth, T. J.: Penetration of UV irradiance into the global ocean, *J. Geophys. Res.*, 116(C11),  
 974 C11020, 2011.
- 975 Stramska, M.: Observations of oceanic whitecaps in the north polar waters of the Atlantic, *J.*  
 976 *Geophys. Res.*, 108(C3), 3086, doi:10.1029/2002JC001321, 2003.
- 977 Taylor, J. P., Edwards, J. M., Glew, M. D., Hignett, P. and Slingo, A.: Studies with a flexible  
 978 new radiation code. II: Comparisons with aircraft short-wave observations, *Q.J.R. Meteorol.*  
 979 *Soc.*, 122(532), 839–861, doi:10.1002/qj.49712253204, 1996.
- 980 Taylor, K. E., Stouffer, R. J. and Meehl, G. A.: An Overview of CMIP5 and the Experiment

Supprimé: .

Supprimé: .

983 Design, Bull. Amer. Meteor. Soc., doi:10.1175/BAMS-D-11-00094.1, 2011.

984 Voldoire, A., Sanchez-Gomez, E., Salas y Mélia, D., Decharme, B., Cassou, C., Sénési, S.,  
985 Valcke, S., Beau, I., Alias, A., Chevallier, M., Déqué, M., Deshayes, J., Douville, H.,  
986 Fernandez, E., Madec, G., Maisonnave, E., Moine, M. P., Planton, S., Saint-Martin, D.,  
987 Szopa, S., Tyteca, S., Alkama, R., Belamari, S., Braun, A., Coquart, L. and Chauvin, F.: The  
988 CNRM-CM5.1 global climate model: description and basic evaluation, *Climate Dynamics*,  
989 40(9-10), 2091–2121, doi:10.1007/s00382-011-1259-y, 2013.

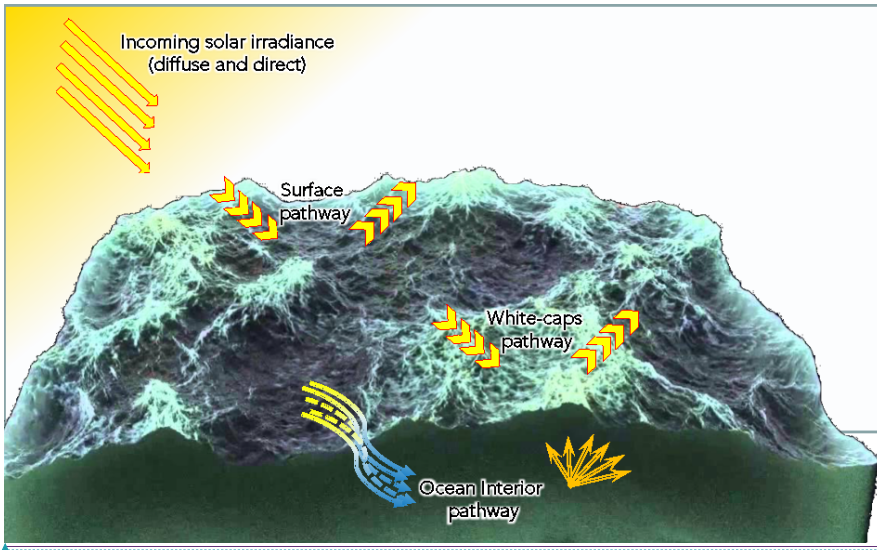
990 Whitlock, C. H., Bartlett, D. S. and Gurganus, E. A.: Sea foam reflectance and influence on  
991 optimum wavelength for remote sensing of ocean aerosols, *Geophys. Res. Lett.*, 9(6), 719–  
992 722, doi:10.1029/GL009i006p00719, 1982.

993 Wielicki, B. A., Barkstrom, B. R., Harrison, E. F., Lee, R. B., III, Louis Smith, G. and  
994 Cooper, J. E.: Clouds and the Earth's Radiant Energy System (CERES): An Earth Observing  
995 System Experiment. *Bull. Amer. Meteor. Soc.*, 77(5), 853–868, doi:10.1175/1520-  
996 0477(1996)077<0853:CATERE>2.0.CO;2, 1996.

997 Woolf, D. K.: Effect of wind waves on air–sea gas exchange: proposal of an overall CO<sub>2</sub>  
998 transfer velocity formula as a function of breaking-wave parameter, *Tellus B*, 57(2), 478–487,  
999 doi:10.1023/A:1021215904955, 2005.

1000 Yoder, J., McClain, C., Feldman, G. and Esaias, W.: Annual Cycles of Phytoplankton  
1001 Chlorophyll Concentrations in the Global Ocean - a Satellite View, *Global Biogeochem.*  
1002 *Cycles*, 7(1), 181–193, doi:10.1029/93GB02358, 1993.

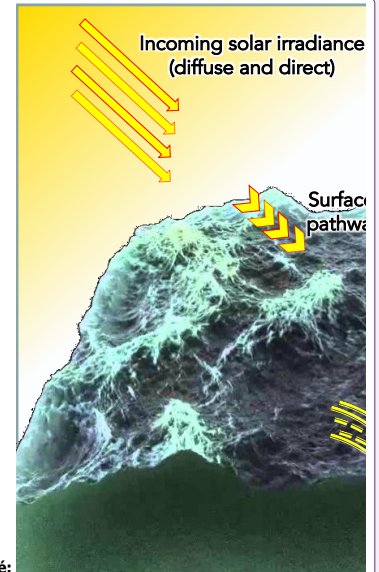
1003  
1004  
1005  
1006  
1007  
1008  
1009  
1010  
1011  
1012  
1013  
1014  
1015  
1016  
1017  
1018



1019  
 1020  
 1021  
 1022  
 1023  
 1024  
 1025  
 1026

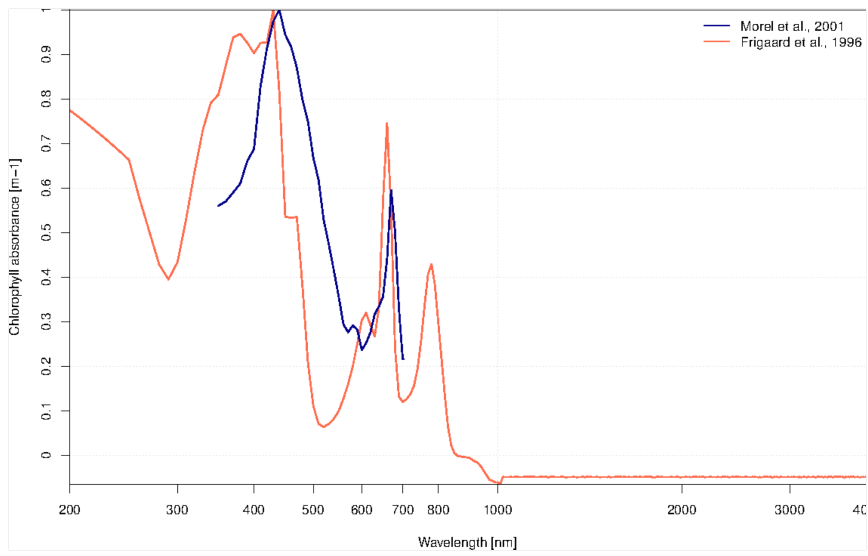
**Figure 1:** Pathways of solar radiation over oceans as described in the new interactive scheme. Whitecaps, surface Fresnel or ocean interior influence of the reflection or the refraction of both direct and diffuse radiation.

Mis en forme: Police : (par défaut) Times, Couleur de police : R,V,B (29,27,28)



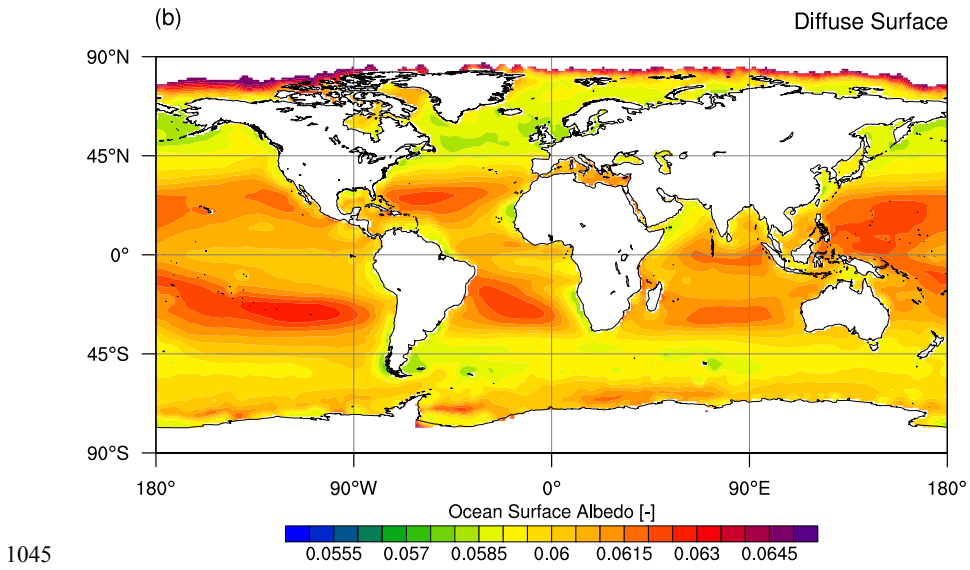
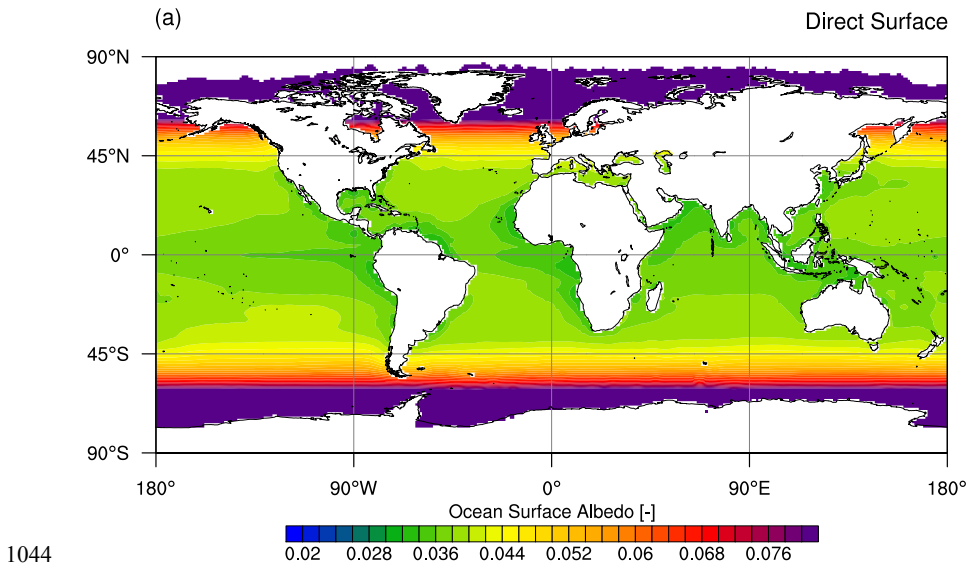
Supprimé:

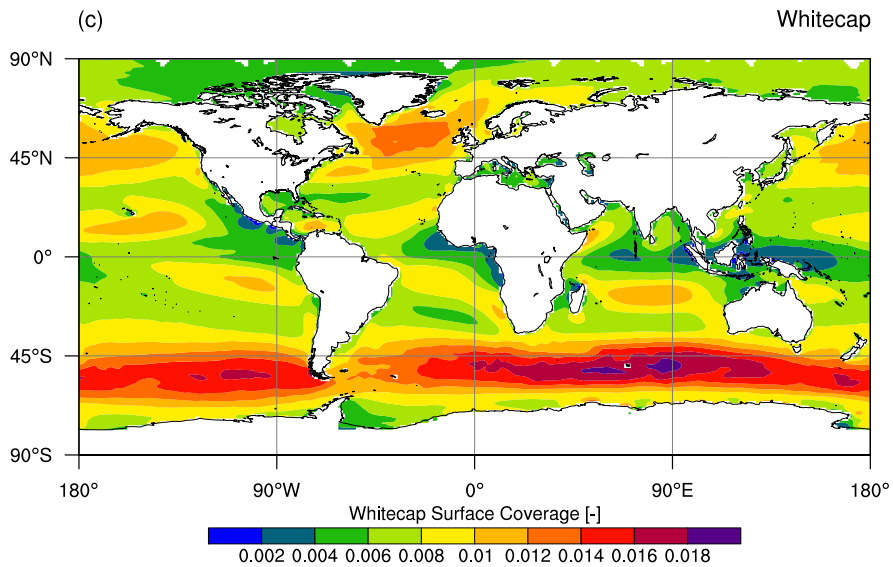
Supprimé: below-water



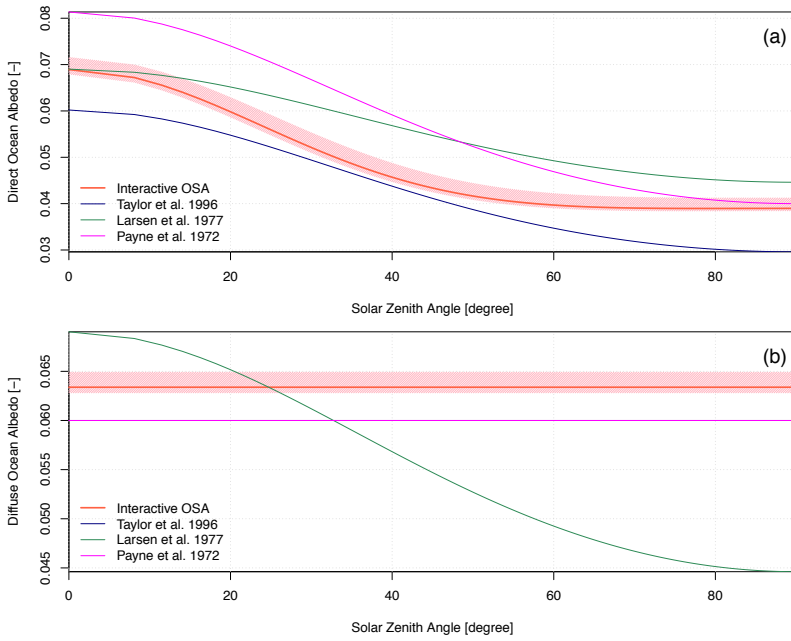
1029  
 1030 **Figure 2:** Comparison of chlorophyll absorbance ( $m^{-1}$ ) as a function of wavelength (nm, in  
 1031 log-scale) from Morel and Maritorea (2001) in blue to that of Frigaard et al. (1996) in red,  
 1032 which is used in the new interactive OSA scheme.

1033  
 1034  
 1035  
 1036  
 1037  
 1038  
 1039  
 1040  
 1041  
 1042  
 1043

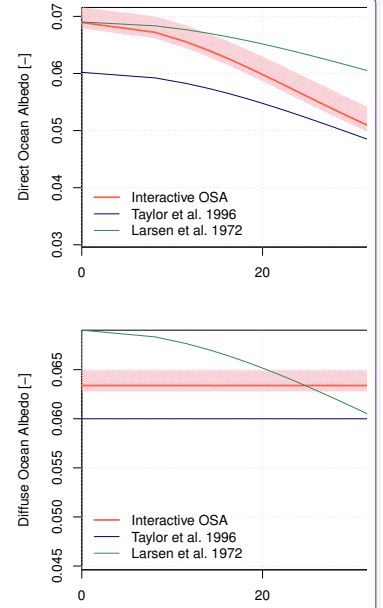




1046  
 1047 **Figure 3:** Maps of ocean surface albedo for (a) direct and (b) diffuse radiation in the absence  
 1048 of whitecaps, and map of whitecaps surface coverage (c). Estimates are derived from offline  
 1049 calculation using EraInterim forcings fields (Dee et al., 2011) from years 2000 to 2012 and  
 1050 SeaWiFS chlorophyll climatology (Siegel et al., 2002) over year 1998-2007. Whitecap albedo  
 1051 is constant in space and is equate to 0.174.  
 1052  
 1053



Mis en forme: Police :(par défaut) Times, Couleur de police : R,V,B (29,27,28)



Supprimé:

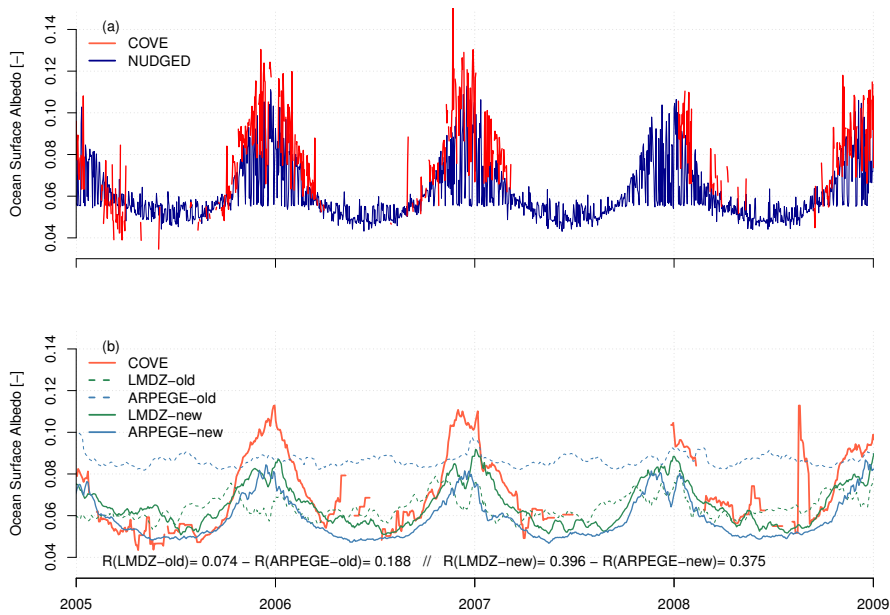
1054

1055 **Figure 4:** Analytical solution for (a) direct and (b) diffuse ocean surface albedo as used in  
 1056 Taylor et al. (1996) and Larsen and Barkstrom (1977), and computed solution for the new  
 1057 interactive ocean surface albedo scheme, as a function of solar zenith angle. [Analytical](#)  
 1058 [solution for direct and diffuse ocean surface albedo as derived from Payne \(1972\) formulation](#)  
 1059 [are also represented in both panels, because this parameterization is currently used in numbers](#)  
 1060 [of state-of-the-art atmospheric and ocean models.](#) Hatching depicts potential variations related  
 1061 to changes in 10-meter wind speed and surface chlorophyll.

1062

1063





1065

1066 **Figure 5:** Ocean surface albedo at COVE station (36.905°N, 75.713°W) from 2005 to 2009.

1067 Panel (a) compares daily-mean time series of ocean surface albedo as derived from ground-

1068 based observations (in red) and as reconstructed with ARPEGE-Climat nudged toward

1069 EraInterim (dark blue). Panel (b) displays, for the sake of clarity, time series of daily-mean

1070 Ocean surface albedo smoothed using a 5-day moving average for both observations and

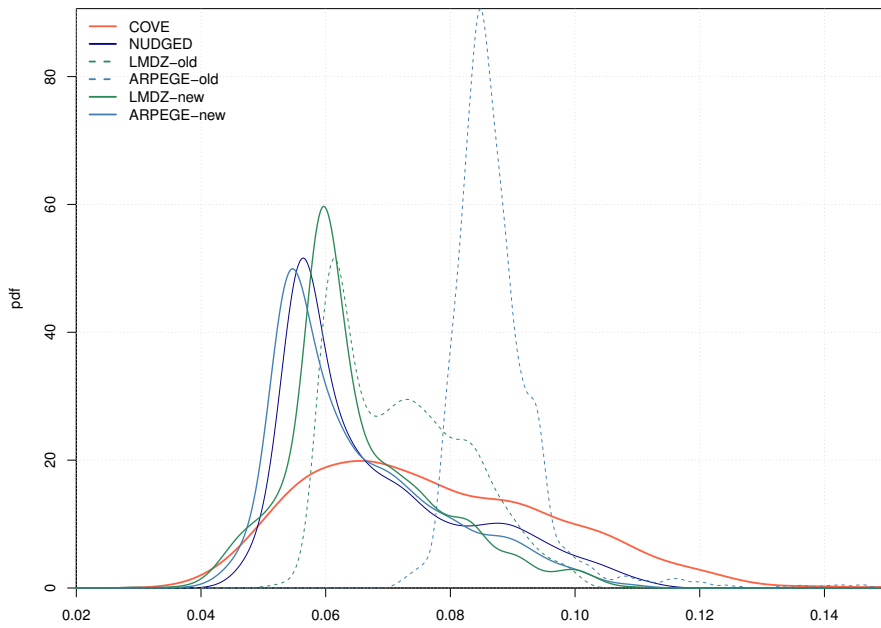
1071 model results. All daily-mean time-series from 2001 to 2015 are displayed in Figure S1.

1072 Ocean surface albedo simulated by ARPEGE-Climat (in blue) and LMDZ (in green) using old

1073 or the new interactive scheme are indicated with dashed or solid lines, respectively.

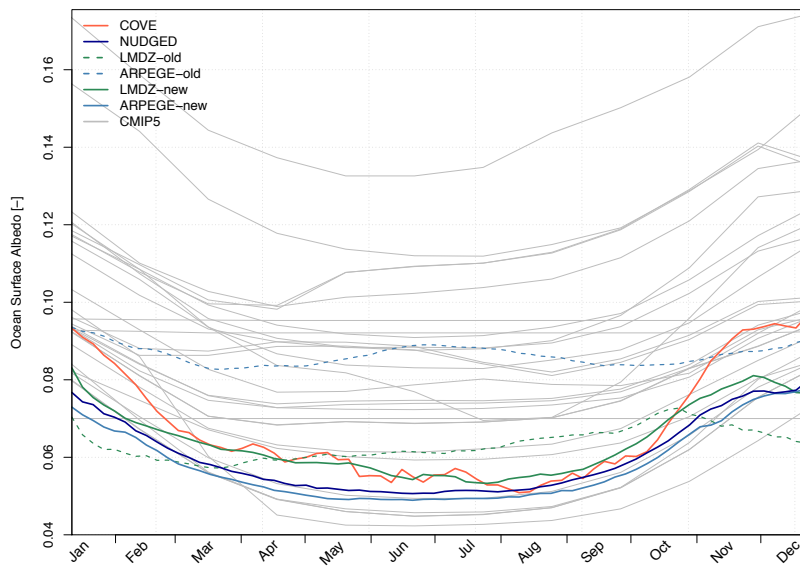
1074

1075



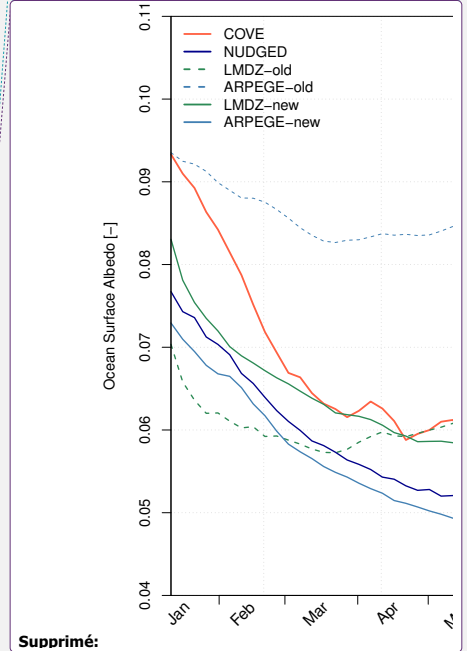
1076  
 1077 **Figure 6:** Probability density function of daily-mean ocean surface albedo at COVE station  
 1078 (36.905°N, 75.713°W) derived from daily-mean time series over years 2001 to 2013. Ocean  
 1079 surface albedo derived from ground-based observations and as reconstructed with ARPEGE-  
 1080 Climat nudged toward ERA-Interim are indicated in red and dark blue, respectively. Ocean  
 1081 surface albedo simulated by ARPEGE-Climat (in blue) and LMDZ (in green) using old or the  
 1082 new interactive scheme are indicated with dashed or solid lines, respectively.

1083  
 1084

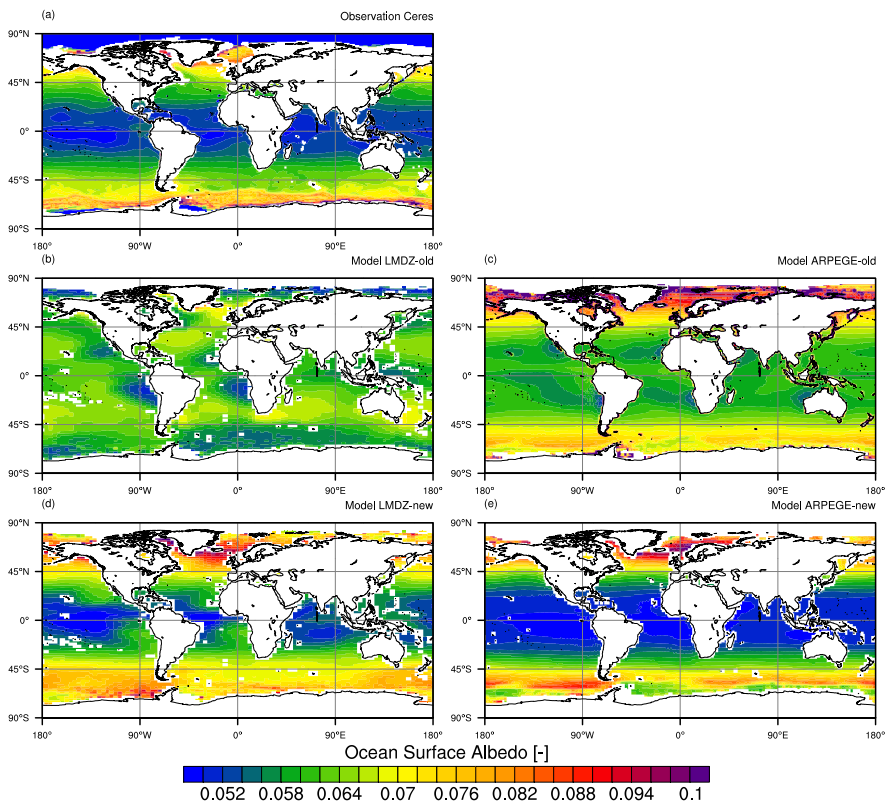


1085  
 1086 **Figure 7:** Mean seasonal cycle of ocean surface albedo at COVE station (36.905°N,  
 1087 75.713°W) derived from daily-mean time series over years 2001 to 2013. Ocean surface  
 1088 albedo derived from ground-based observations and as reconstructed with ARPEGE-Climat  
 1089 nudged toward EraInterim are indicated in red and dark blue, respectively. Ocean surface  
 1090 albedo simulated by ARPEGE-Climat (in blue) and LMDZ (in green) using old or the new  
 1091 interactive scheme are indicated with dashed or solid lines, respectively. For comparison, the  
 1092 mean seasonal cycle of ocean surface albedo at COVE as simulated by available CMIP5  
 1093 models is represented by thin grey lines.  
 1094

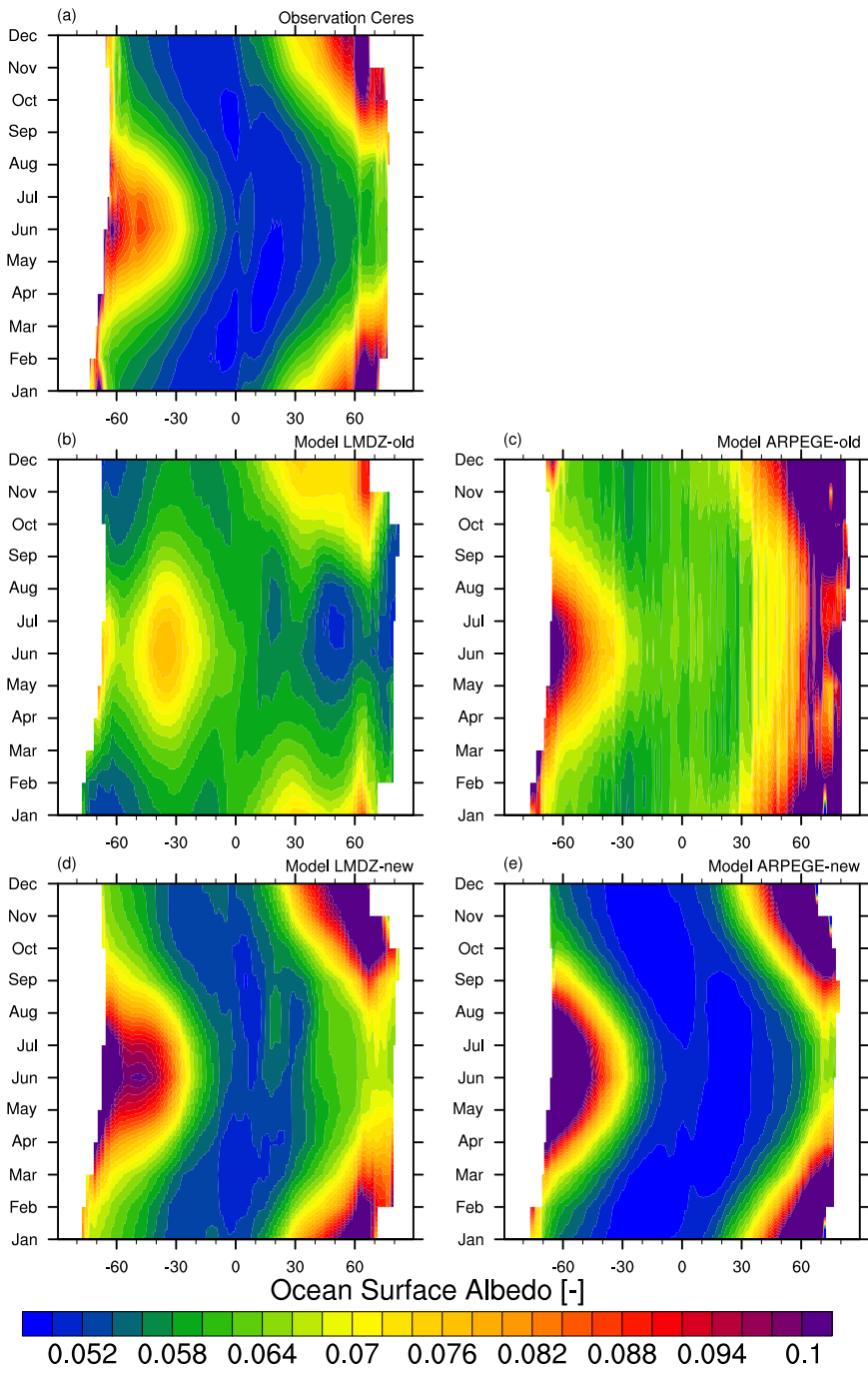
Mis en forme: Police : (par défaut) Times, Couleur de police : R,V,B (29,27,28)



Supprimé:



1096  
 1097 **Figure 8:** Decadal-mean climatology ocean surface albedo as (a) estimated from CERES  
 1098 satellite observations (Wielicki et al., 1996) and as simulated by LMDZ (b,d) and ARPEGE-  
 1099 Climat (c,e). In panels (b) and (c), LMDZ and ARPEGE-Climat use old ocean albedo  
 1100 schemes, that is Taylor et al. (1996) and Larsen and Barkstrom (1977), respectively. In panels  
 1101 (d) and (e), LMDZ and ARPEGE-Climat use employ the new interactive ocean surface albedo  
 1102 scheme. Decadal-mean climatology is derived from radiative fluxes averaged over years 2001  
 1103 to 2014 for CERES estimates and 2000 to 2012 for both climates models.  
 1104



1105

1106 **Figure 9:** Hovmöller diagram representing the zonally-averaged ocean surface albedo as a  
1107 function of month. The various panels display the ocean surface albedo as (a) estimated from  
1108 CERES satellite observations (Wielicki et al., 1996) and as simulated by (b) LMDZ and (c)  
1109 ARPEGE-Climat using old ocean albedo schemes, that is Taylor et al. (1996) and Larsen and  
1110 Barkstrom (1977), respectively. Panels (d) and (e) show OSA as simulated by the new  
1111 interactive ocean surface albedo scheme for LMDZ and ARPEGE-Climat, respectively.  
1112 Monthly-mean are derived from radiative fluxes averaged over years 2001 to 2014 for  
1113 CERES estimates and from years 2000 to 2012 for both climates models.  
1114